

Vorlesung 9:

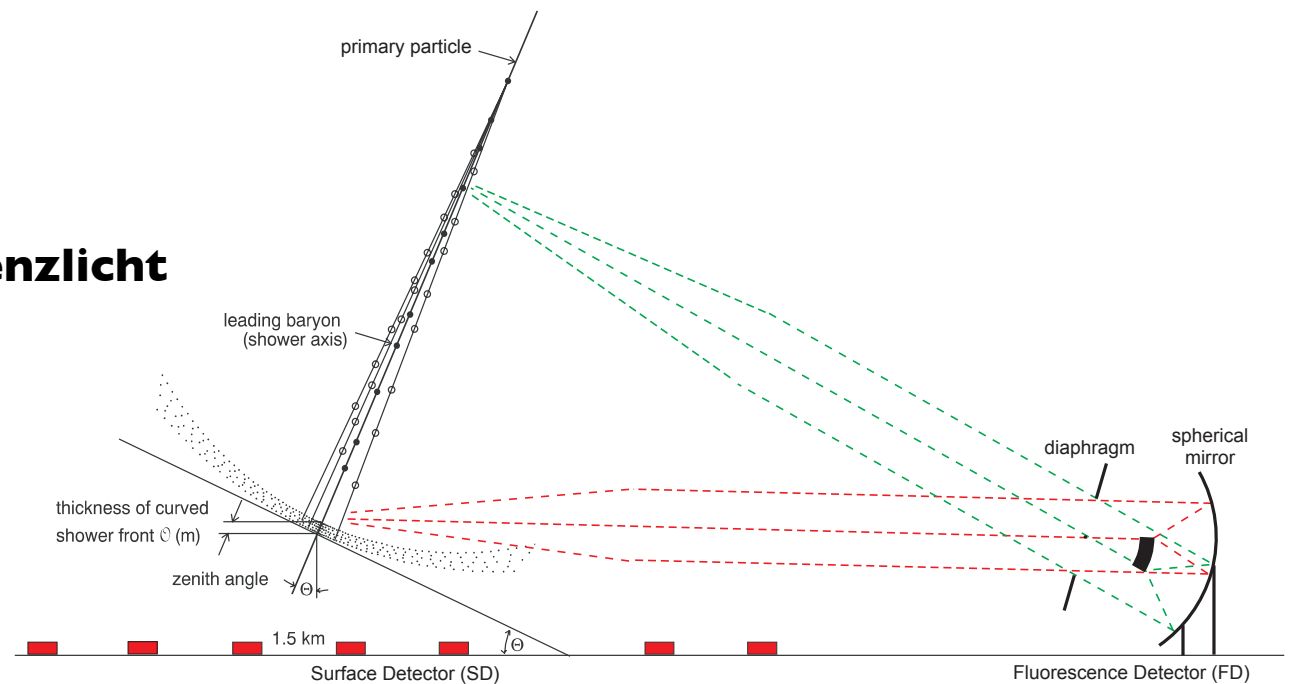
Abschluss: Indirekte Messung kosmischer Strahlung

Kalorimetrische Messung von Schauern mit Fluoreszenzlicht

- Prozess der Fluoreszenzemission in Luft
- Korrektur für nicht nachgewiesene Energie

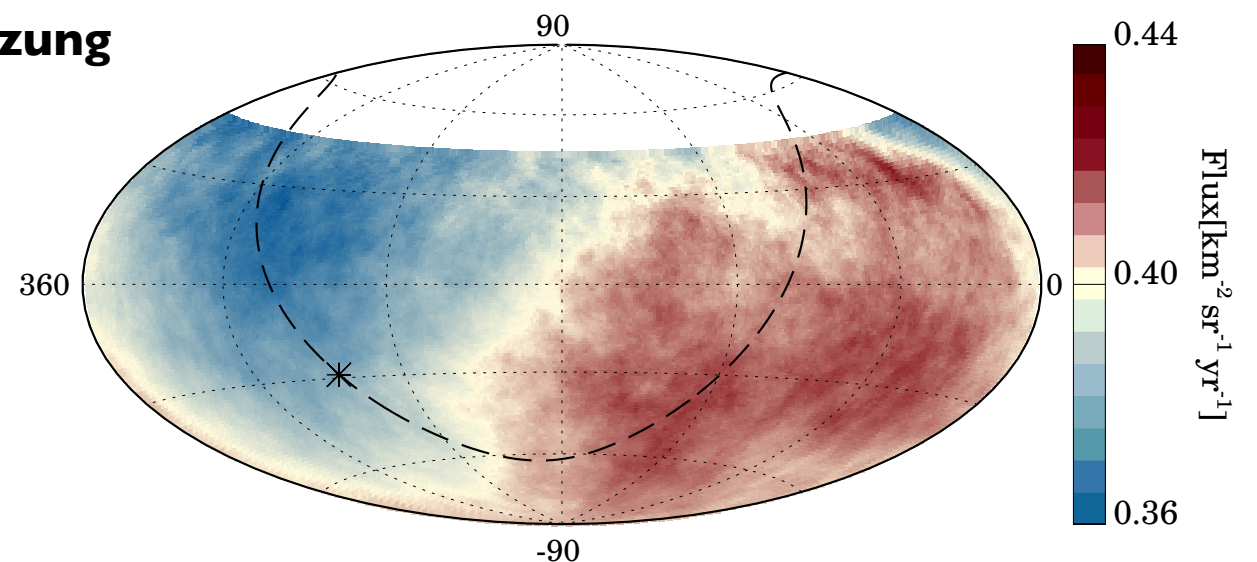
Beispiel: das Pierre Auger-Observatorium

- Aufbau und Schauernachweismethoden
- Methode der Hybrid-Messung



Daten zum Primärfluss und der Elementzusammensetzung

- Knöchel (Ankle) im Fluss: Übergang zu extragalaktischen Quellen?
- Tiefe des Schauernmaximums und Interpretation
- Anisotropie



Vorlesung und Übungen : Daten

Vorlesung: Dienstags

~~3. Nov. 2020~~
~~10. Nov. 2020~~
~~17. Nov. 2020~~
~~24. Nov. 2020~~
~~1. Dez. 2020~~
~~8. Dez. 2020~~
~~15. Dez. 2020~~
~~22. Dez. 2020~~
~~12. Jan. 2021~~
~~19. Jan. 2021~~
~~26. Jan. 2021~~
2. Feb. 2021
4. Feb. 2021
9. Feb. 2021
16. Feb. 2021

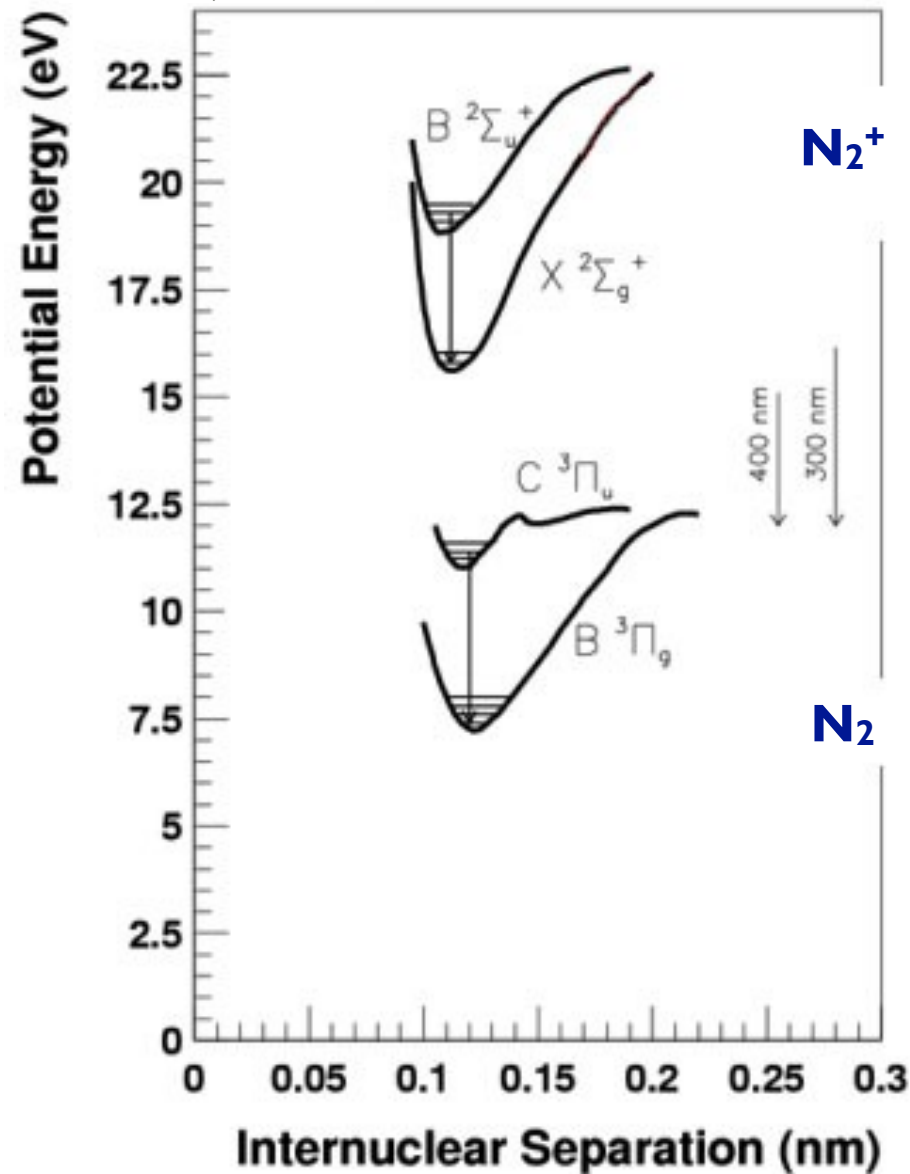
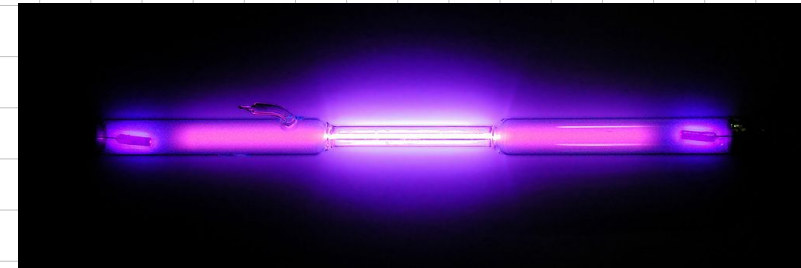
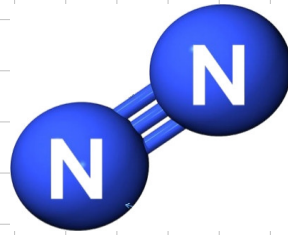
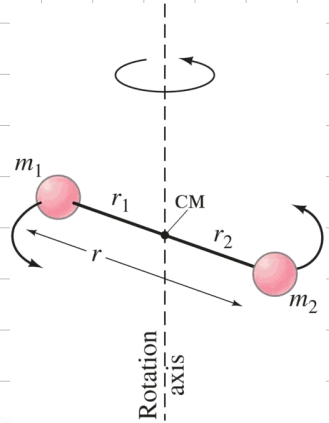
Ersatz für 19.1.

Übungen: Donnerstags

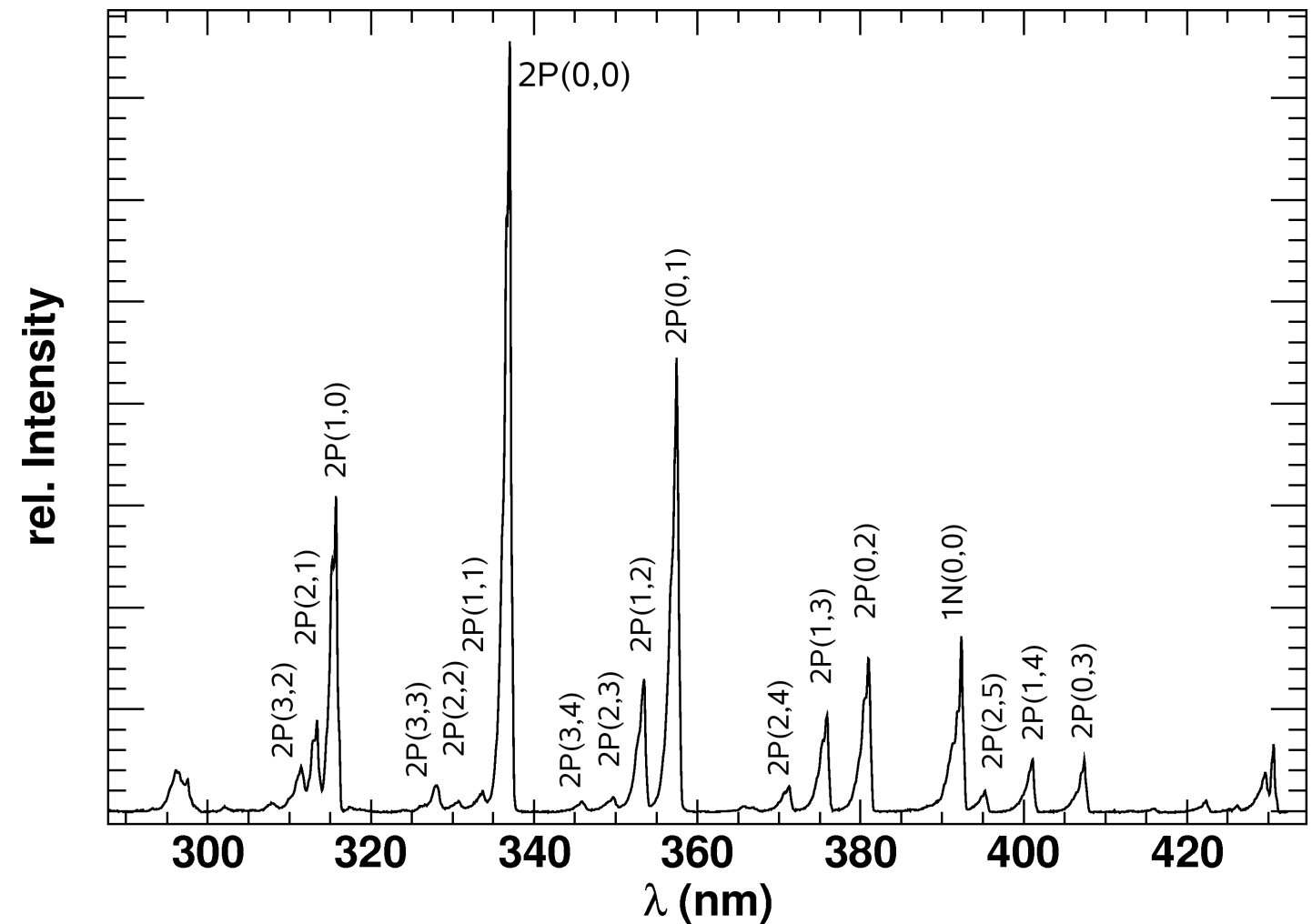
gehalten von Max Stadelmaier

~~19.11.2020 - Blatt 1~~
~~03.12.2020 - Blatt 2~~
~~17.12.2020 - Blatt 3~~
~~14.01.2021 - Blatt 4~~
11.02.2021 - Präsentation (Paul Filip)
18.02.2021 - Blatt 5

Fluoreszenzlicht von Stickstoffmolekülen

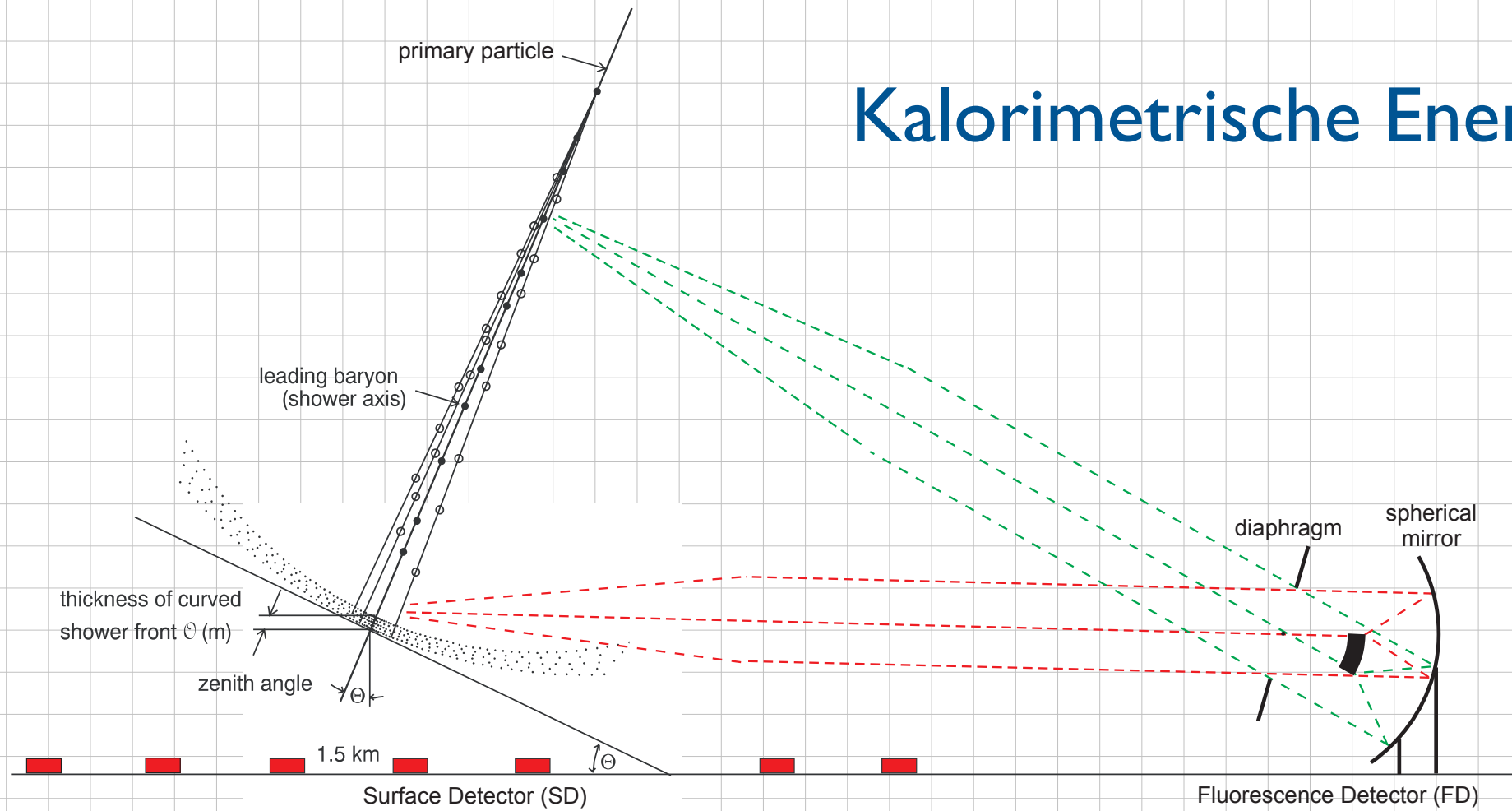


3-4 Photonen/m/Teilchen in 10km Höhe
entspricht einer 30 Watt-Glühbirne

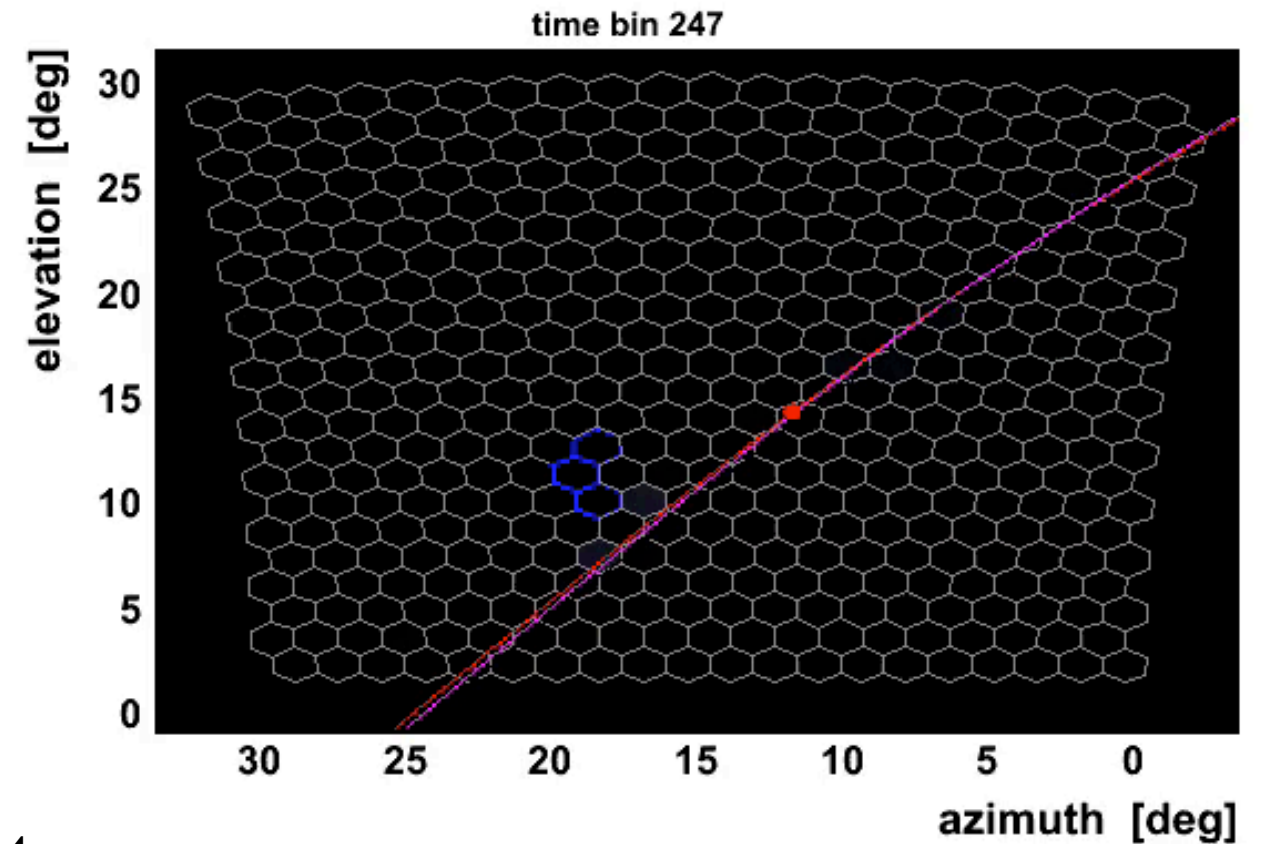
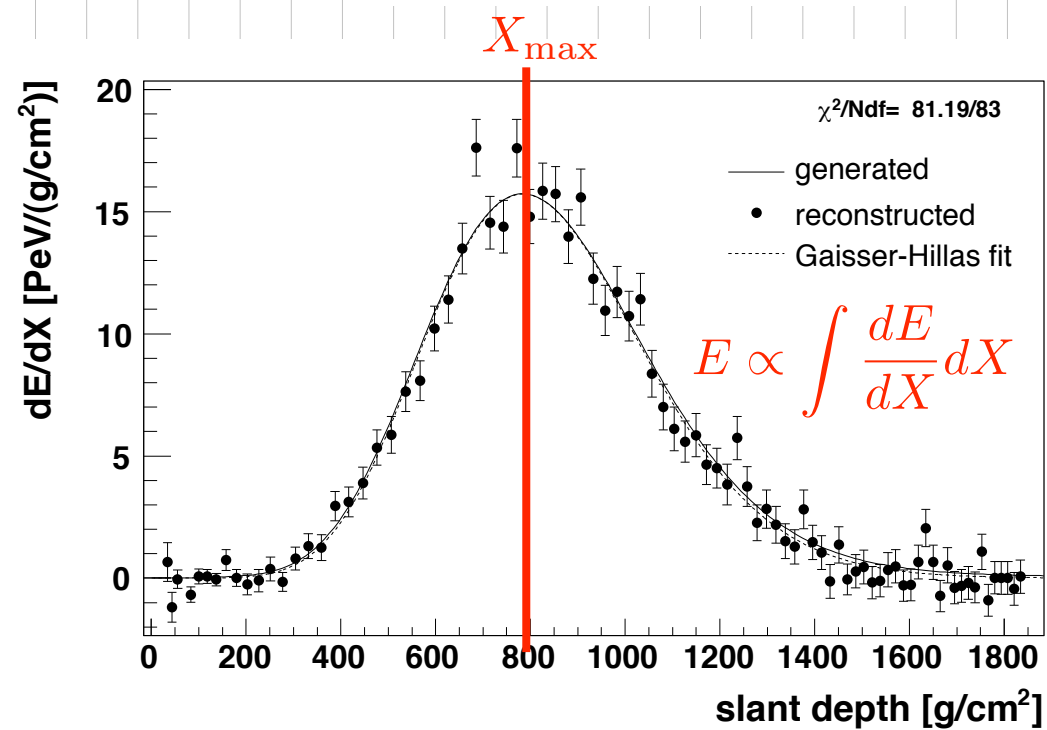


Lebensdauer des angeregten Zustands $\sim 10^{-8} \text{ s} = 10 \text{ ns}$
isotrope Emission, hauptsächlich im UV (300 - 400 nm)

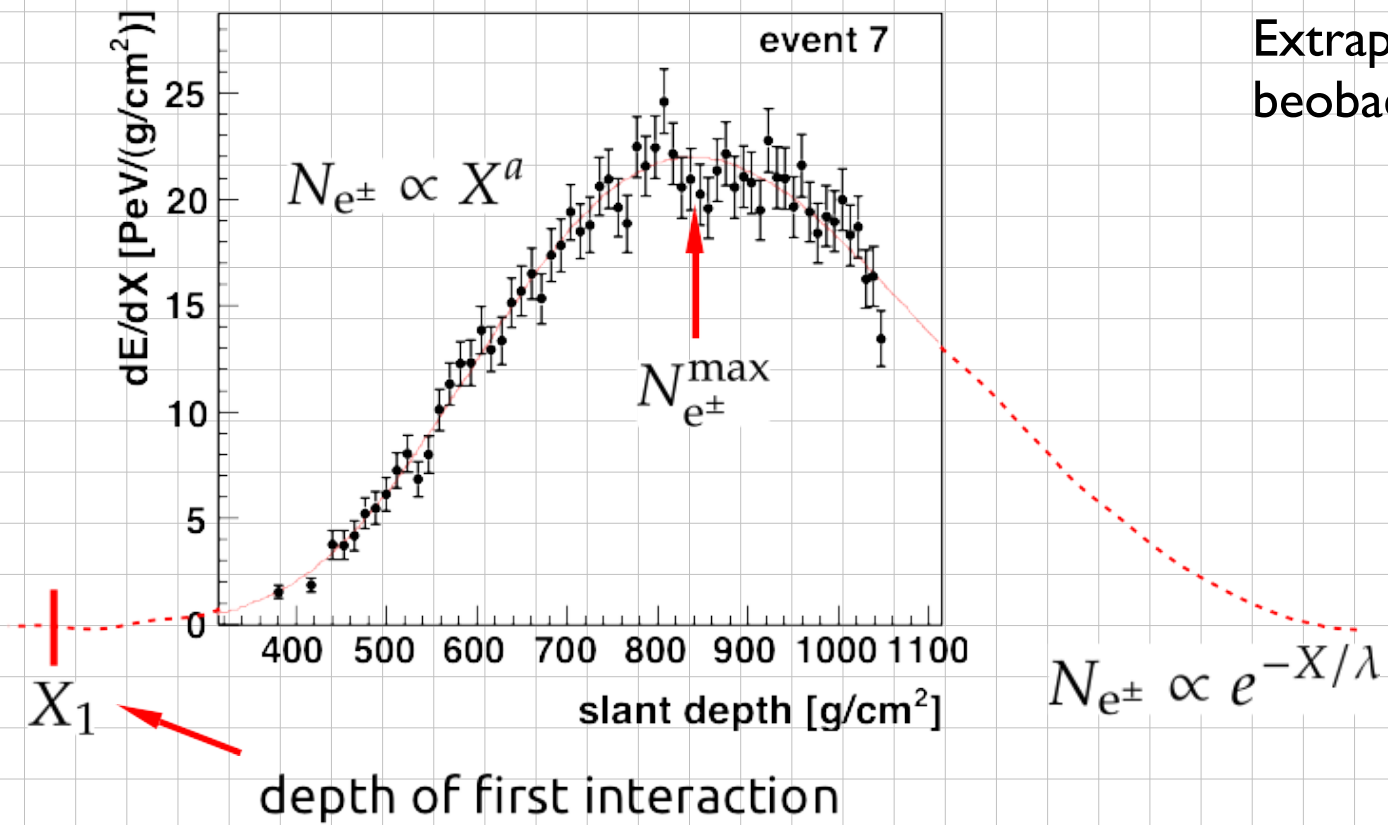
Kalorimetrische Energiemessung



Ionisationsenergieabgabe in Luft



Kalorimetrische Messung der Energie



Extrapolation in nicht direkt beobachtete Bereiche erforderlich

$$E_{\text{cal}} = \int_0^\infty \left(\frac{dE}{dX} \right)_{\text{measured}} dX$$

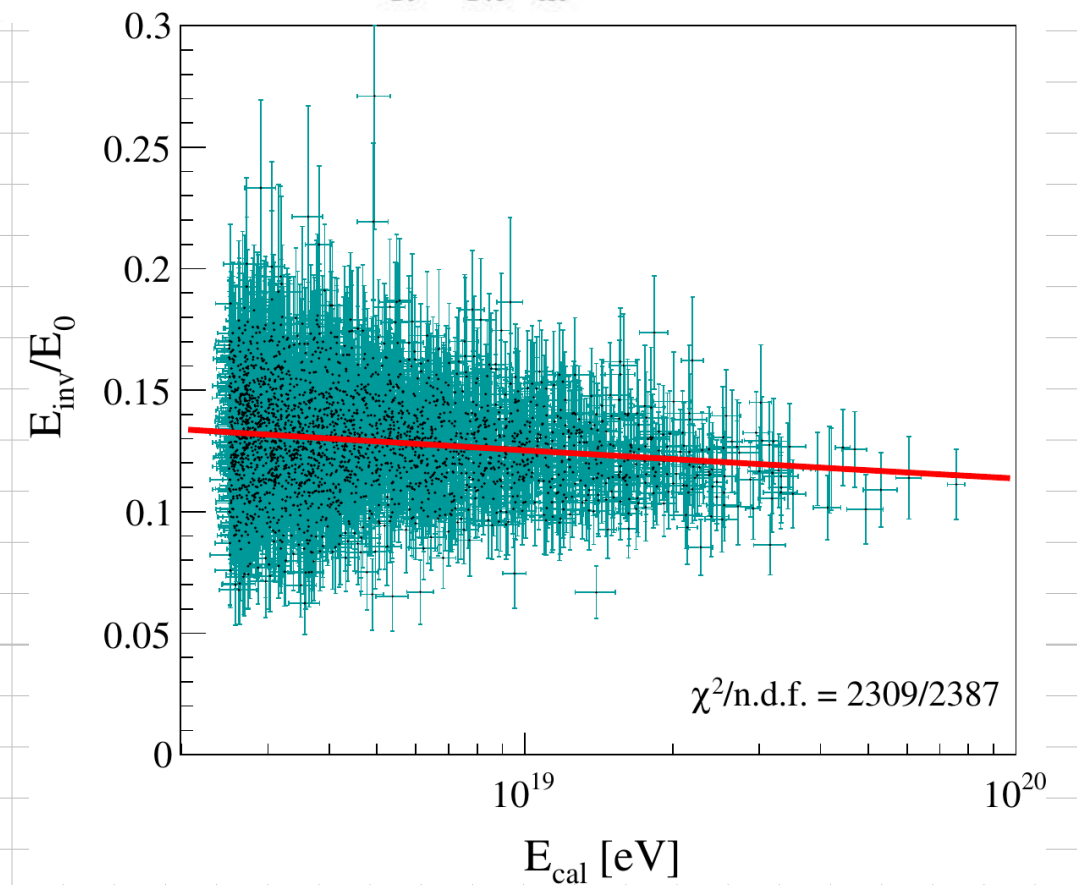
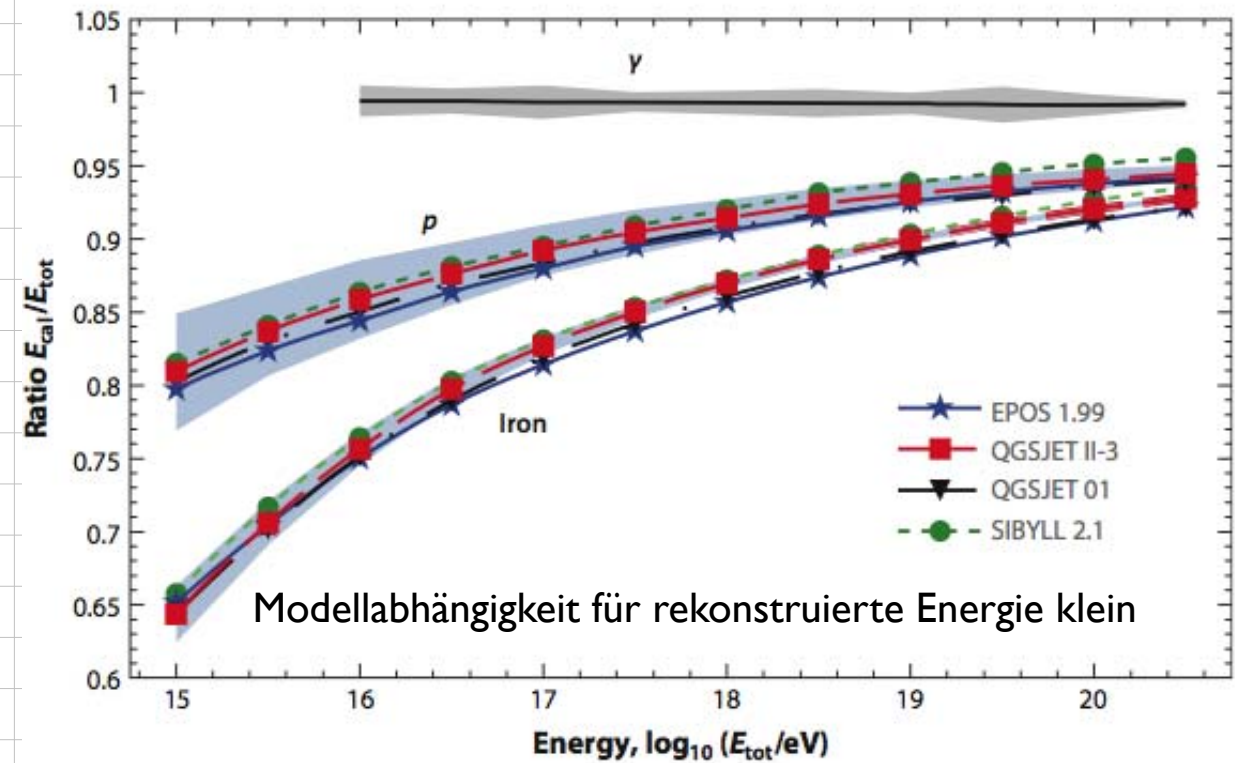
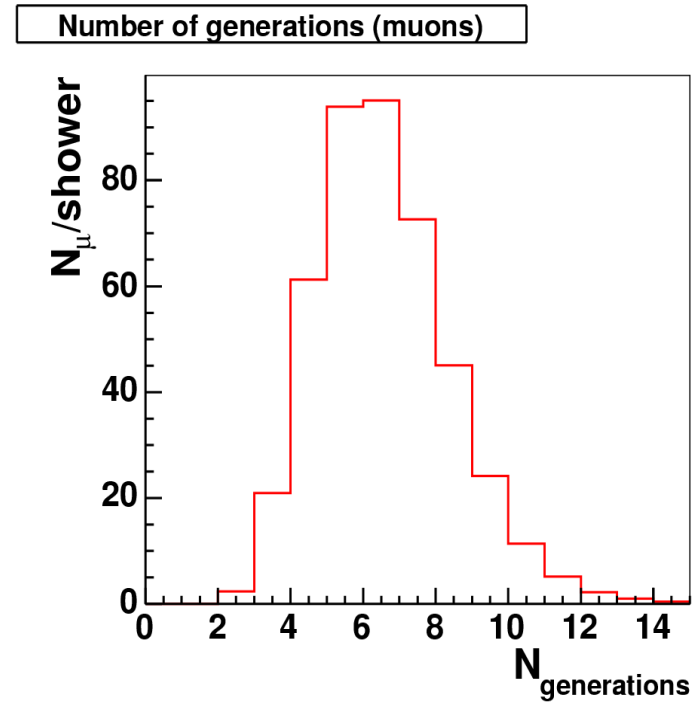
$$\approx \int_0^\infty \langle \alpha_{\text{ion}} \rangle \left(\frac{dN_e}{dX} \right)_{\text{measured}} dX$$

$$N_e(X) = N_{e,\text{max}} \left(\frac{X - X_1}{X_{\text{max}} - X_1} \right)^{\frac{X_{\text{max}} - X_1}{\Lambda}} \exp \left(\frac{X_{\text{max}} - X}{\Lambda} \right)$$

Korrektur der *unsichtbaren Energie*

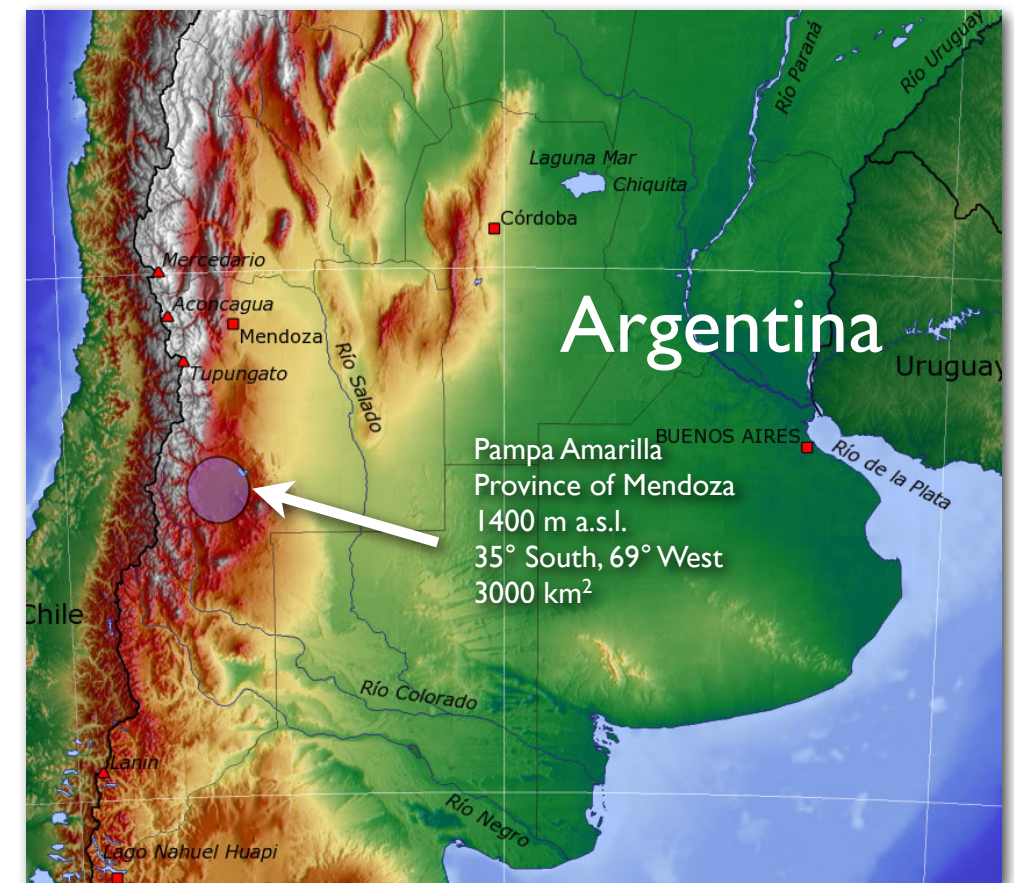
Energiekorrekturfaktor für Fluoreszenzmessungen

Protonschauer, $E = 10^{15}$ eV

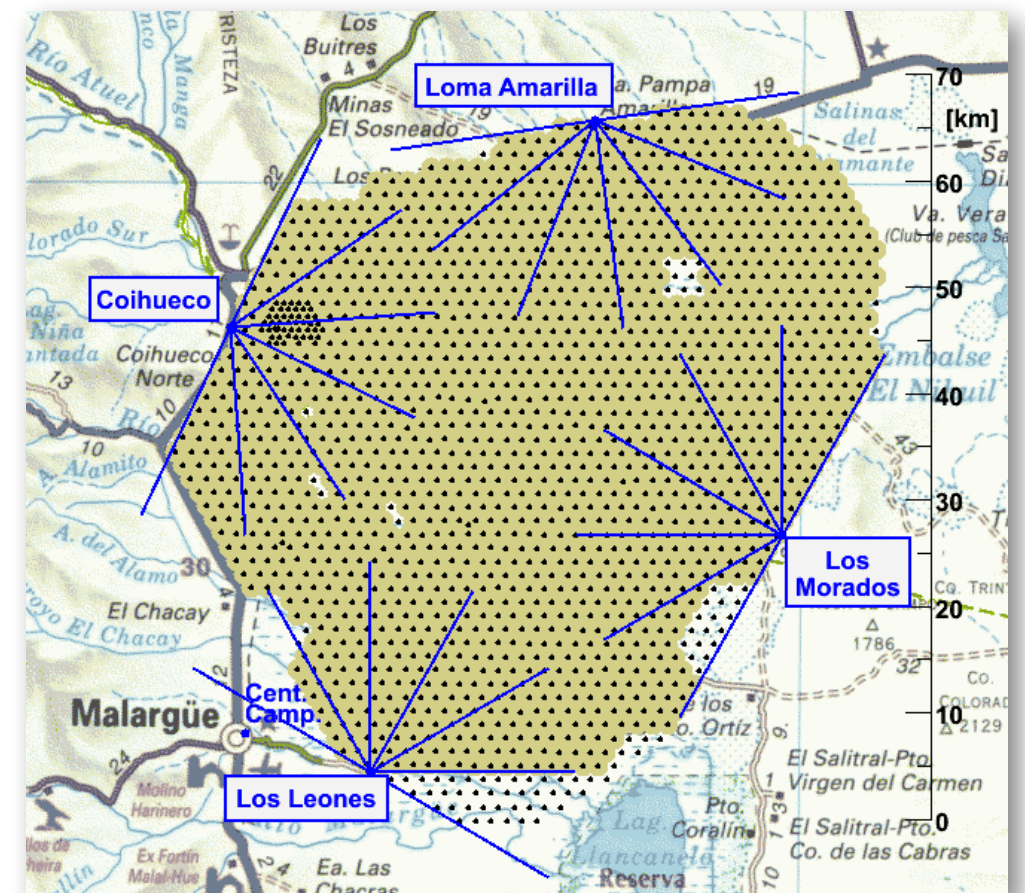


The Pierre Auger Observatory

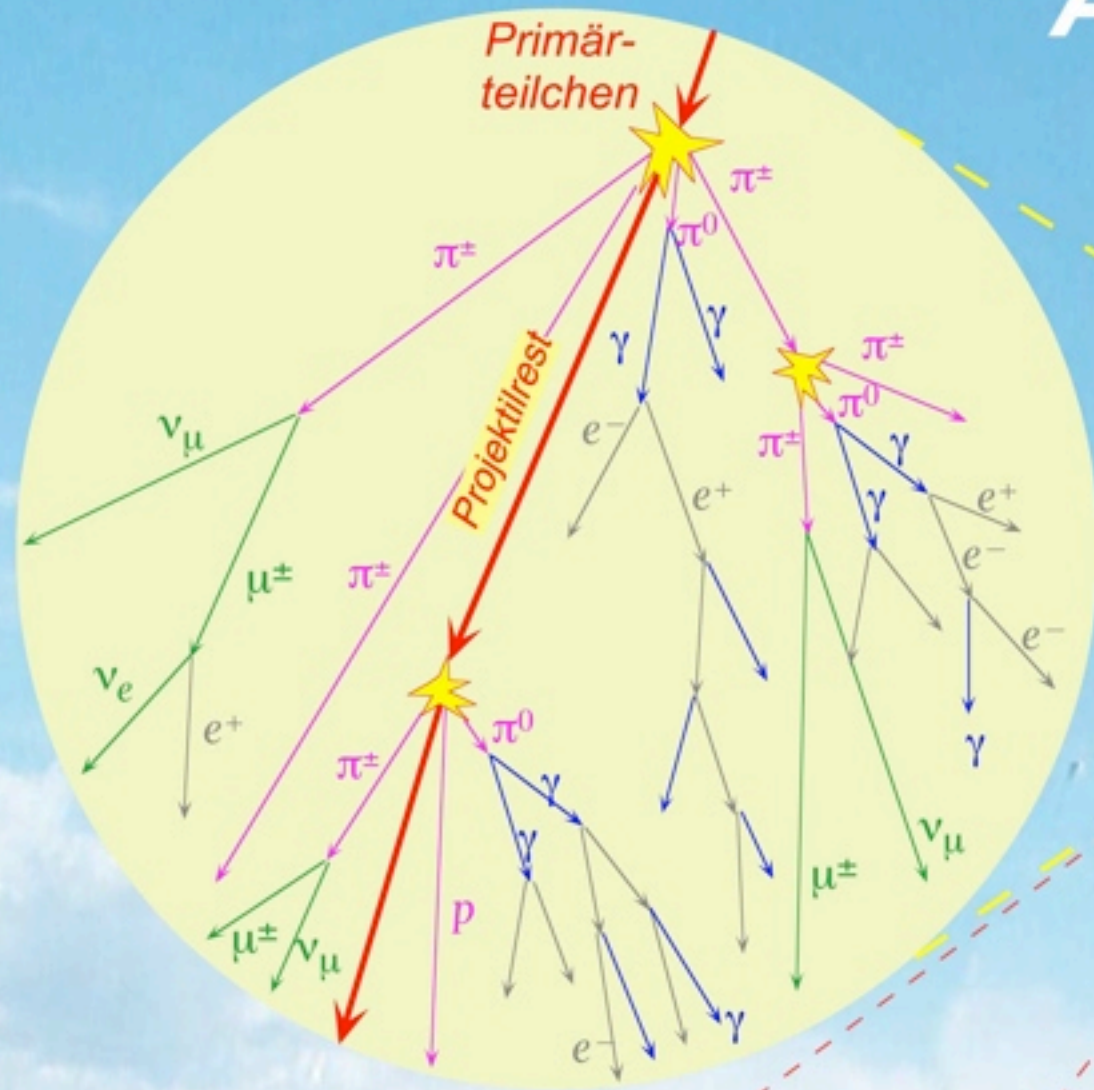
- Auger: >400 authors from 17 countries
- Southern site:
Hybrid detector near Malargüe/Argentina
- June 13th 2008 : 1660 tanks deployed
1637 with water
1603 totally equipped
- All 4 fluorescence buildings complete
each with 6 telescopes since February 2007



3



Ausgedehnte Luftschauer



Pierre Auger Observatorium:
 $10^{19} \text{ eV} < E < 10^{21++} \text{ eV}$

Primärteilchen

ca 8 km Höhe

Fluoreszenz,
Cherenkov Licht

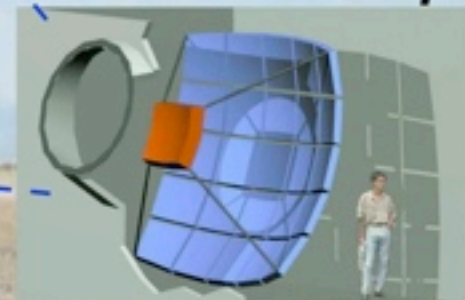
Elektronisches
Schmidt-Teleskop

1 m Dicke

Trajektorie

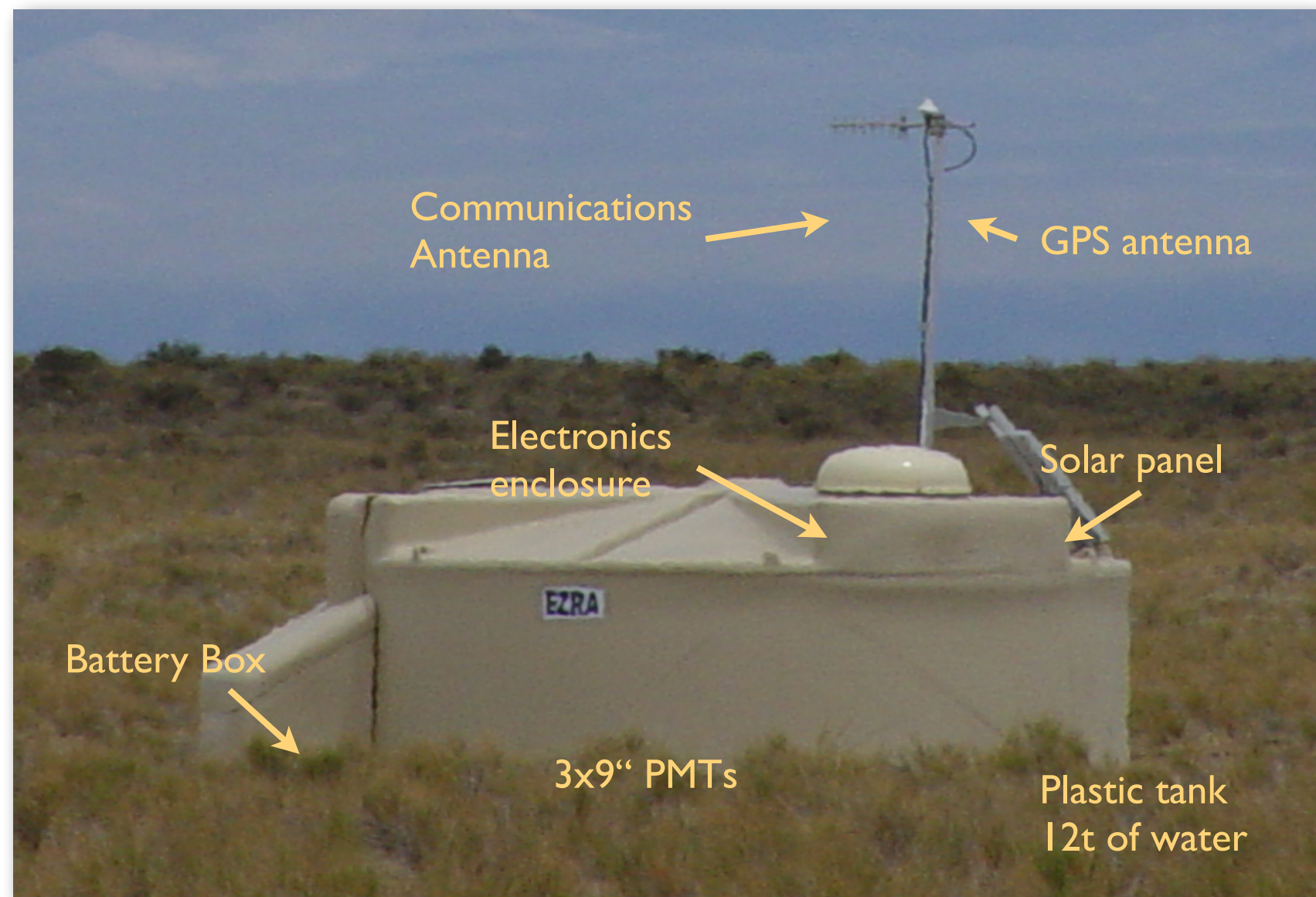
$\gamma \approx c$

Wasser-
Cherenkovdetektoren

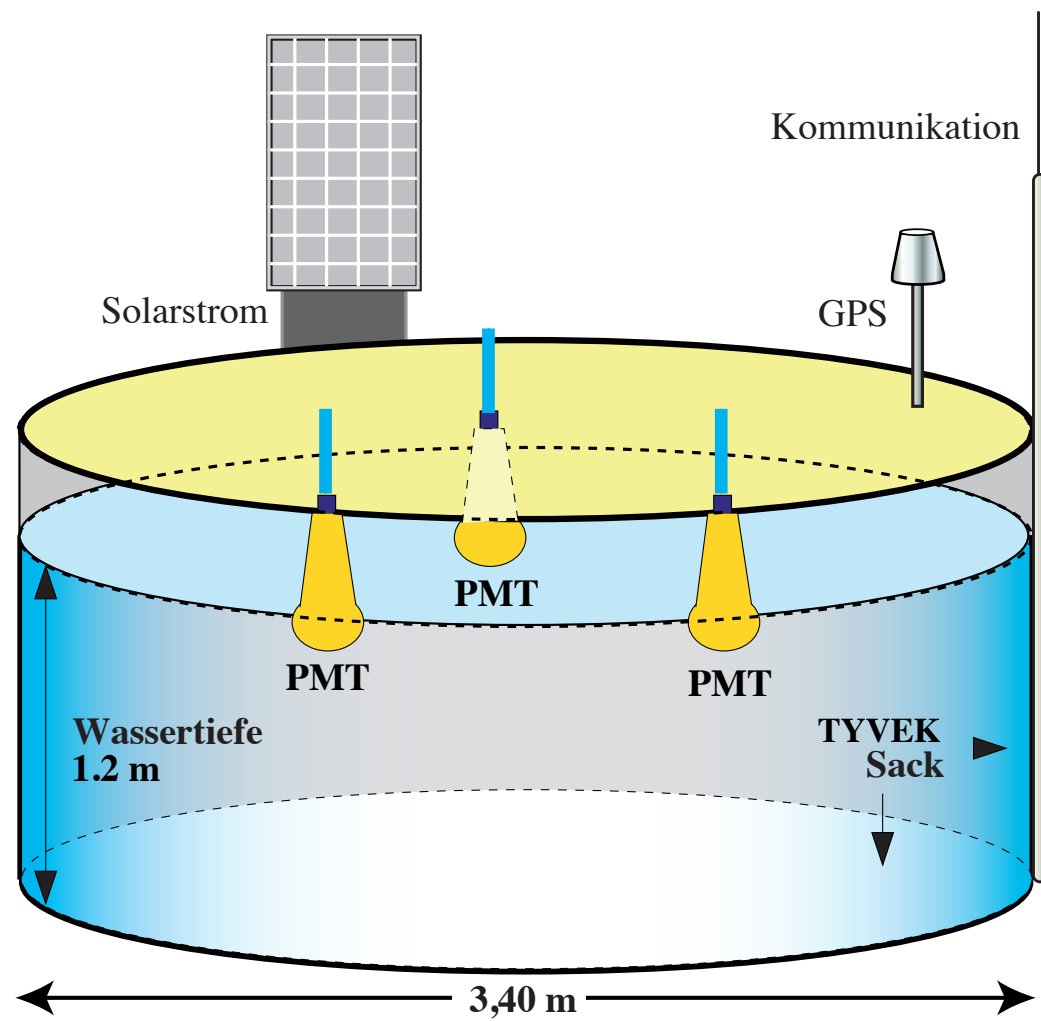


The surface detector

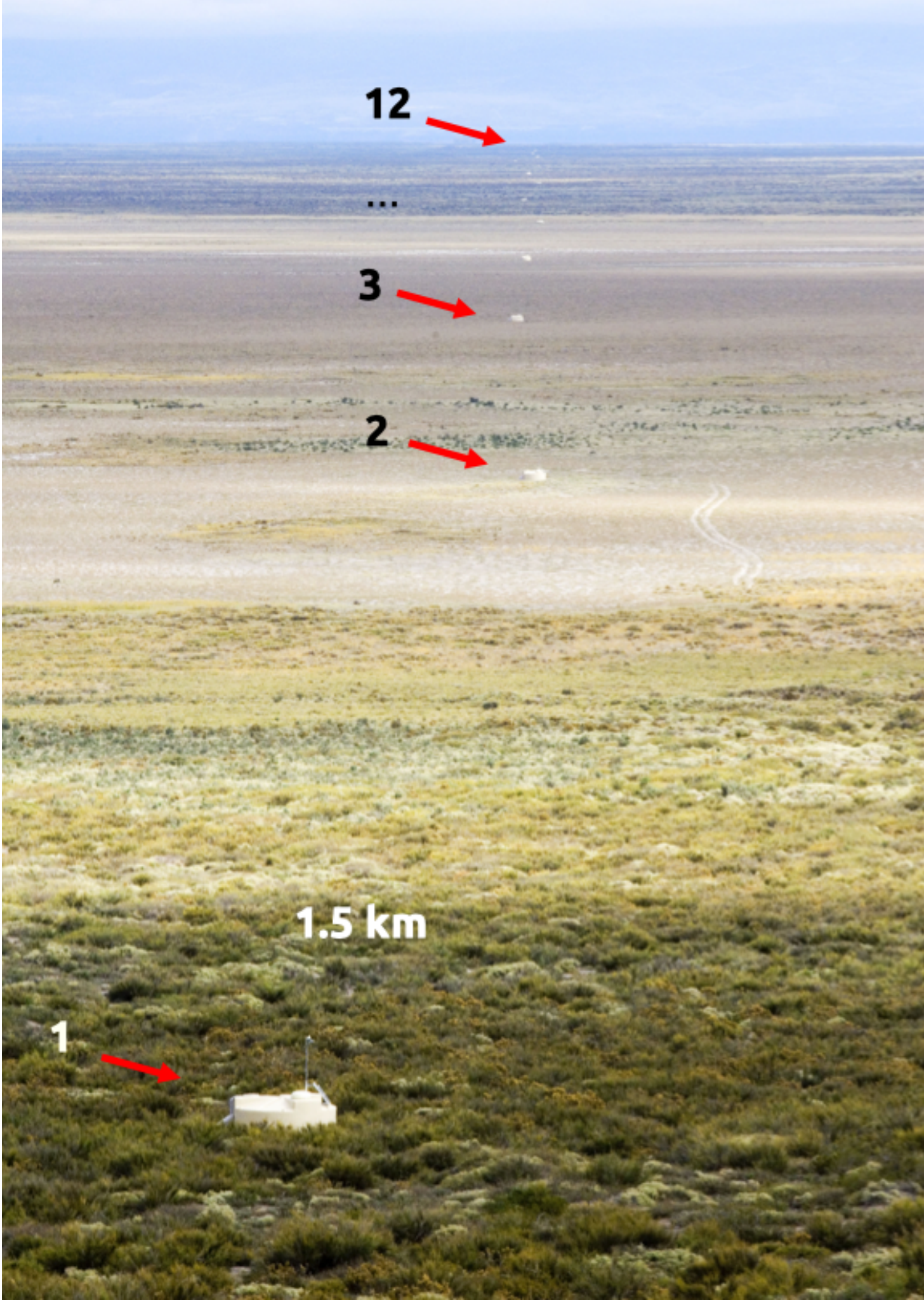
- 1600 Water Cherenkov tanks (1.2 m height, 10 m² area)
- 12,000 ltrs of purified Water
- Three 9" PMTs
- 40 MHz FADCs
- solar powered
- GPS based timing
- micro-wave communication



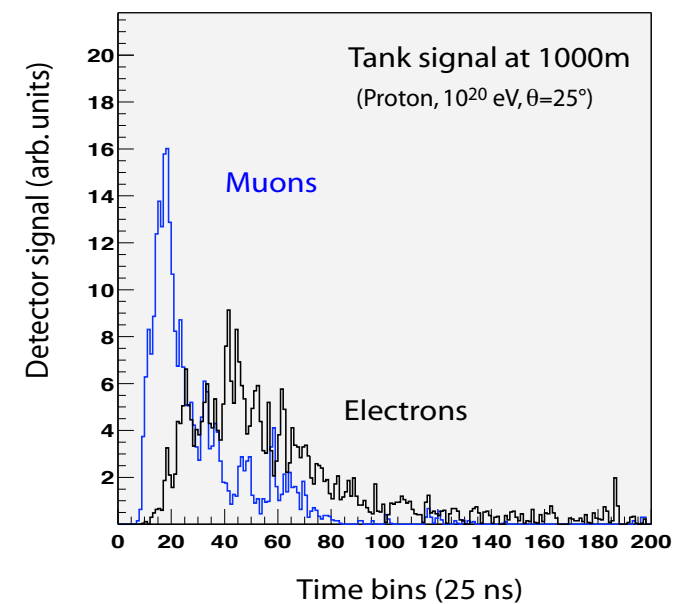
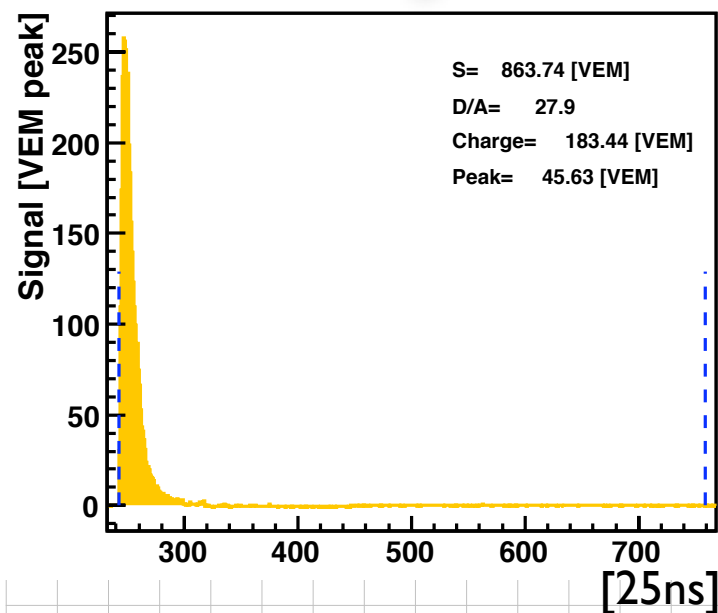
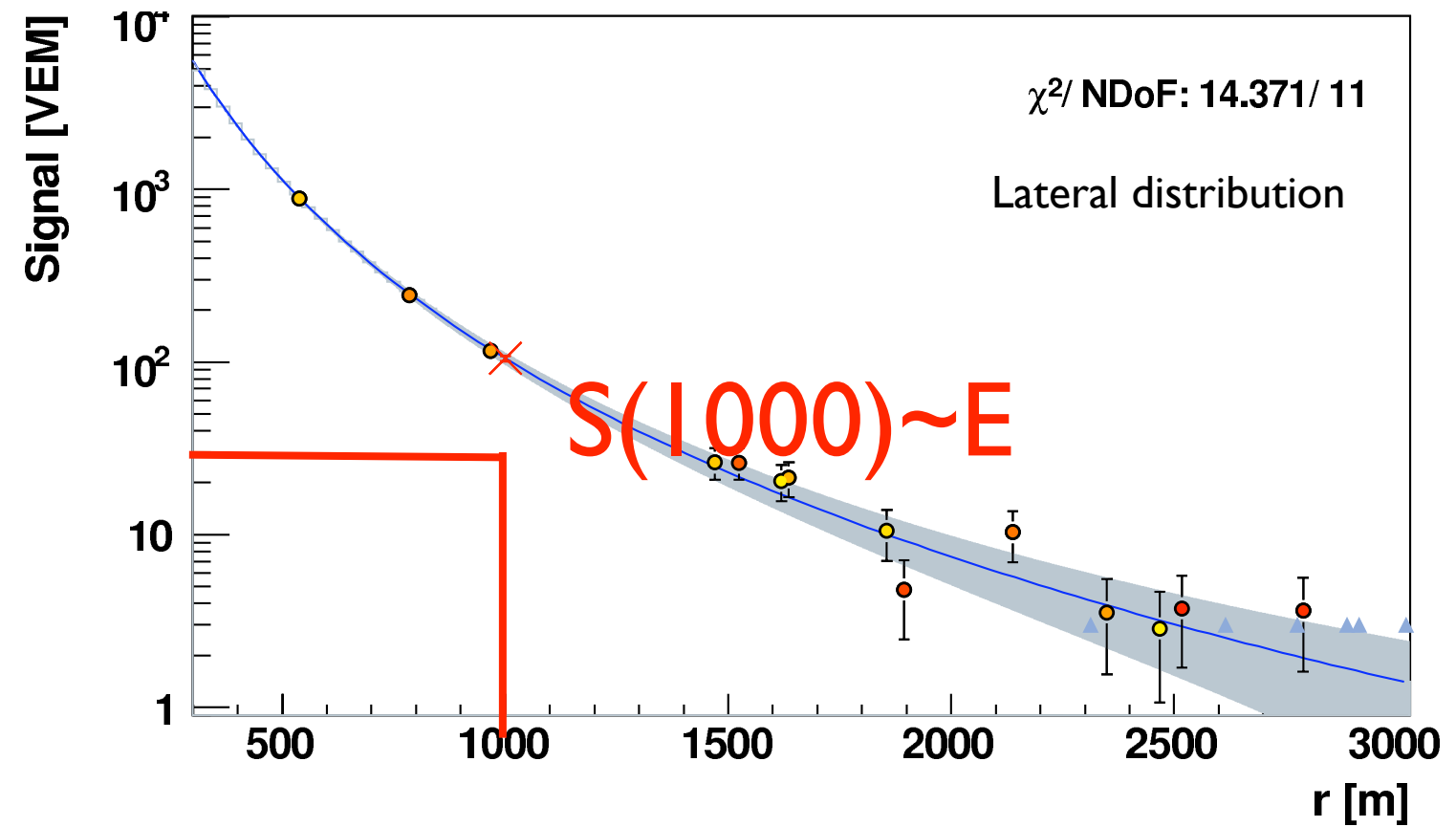
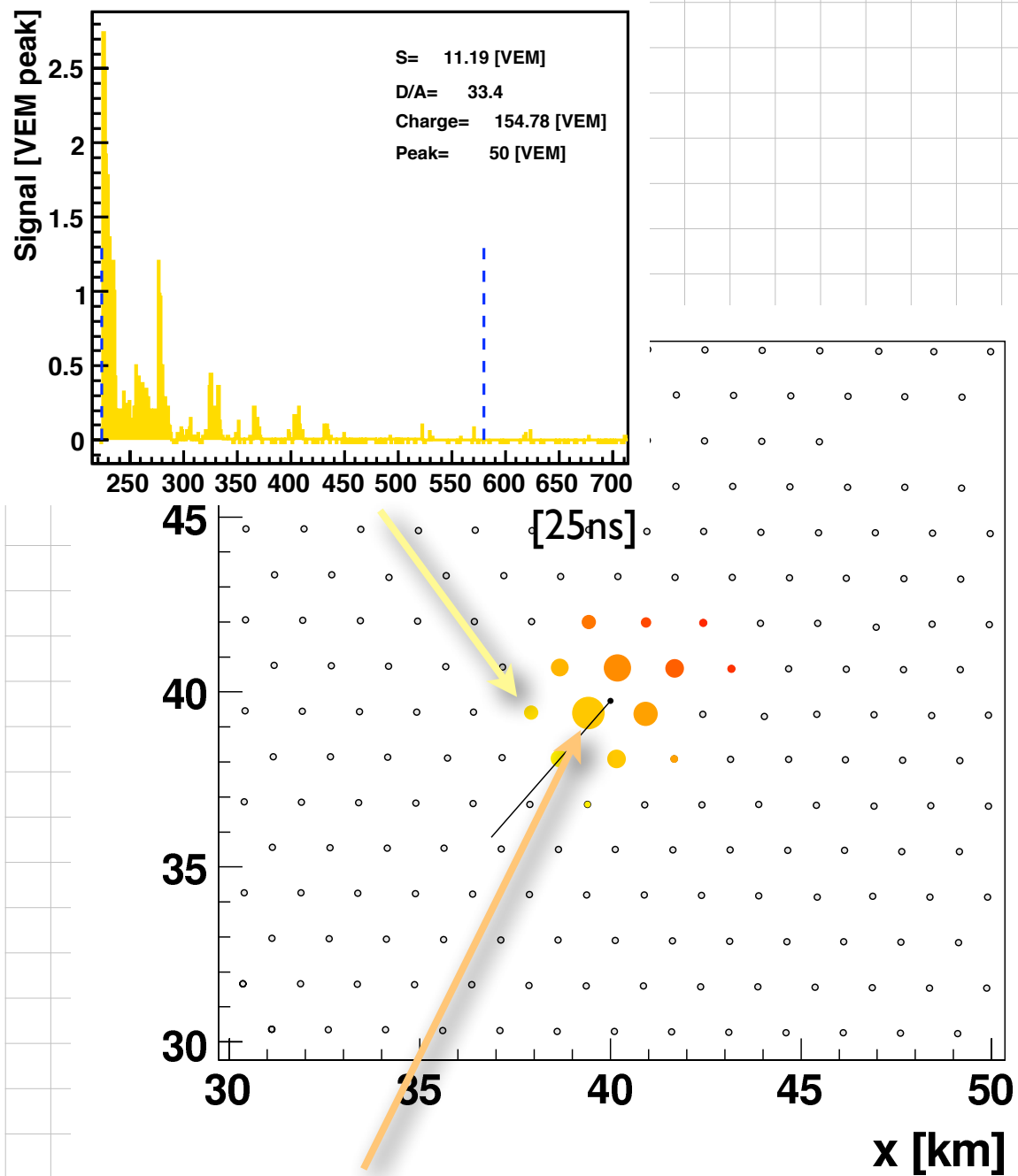
Wasser-Cherenkovdetektor



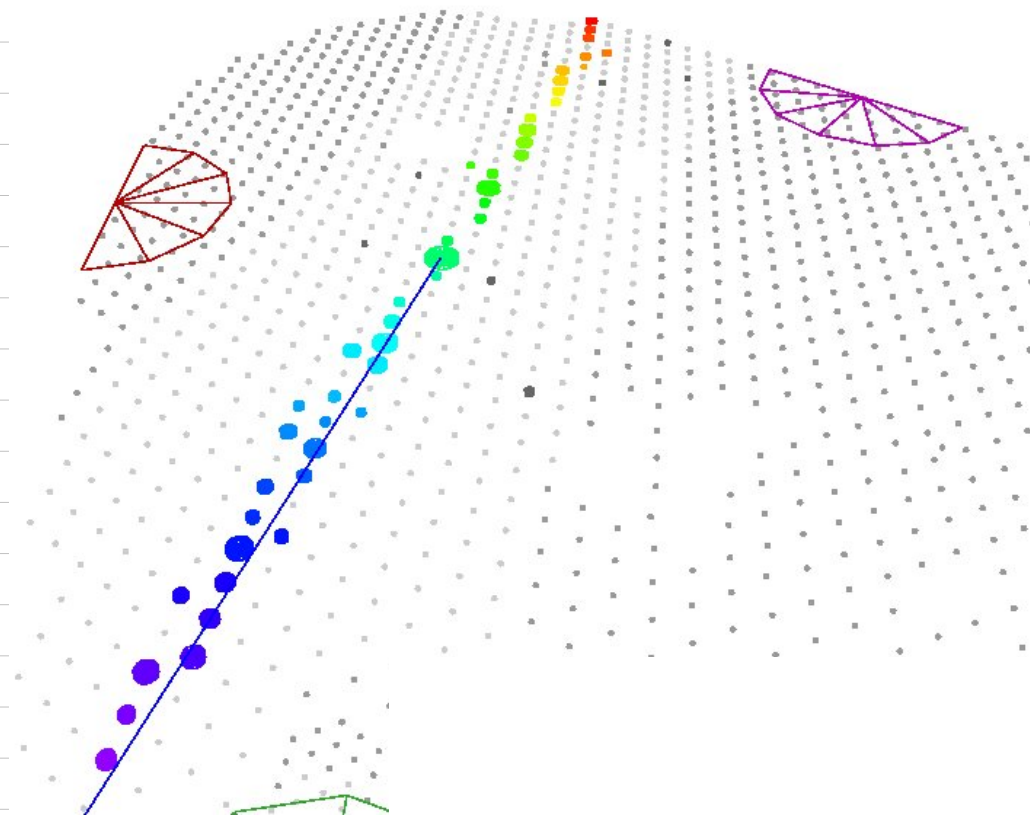




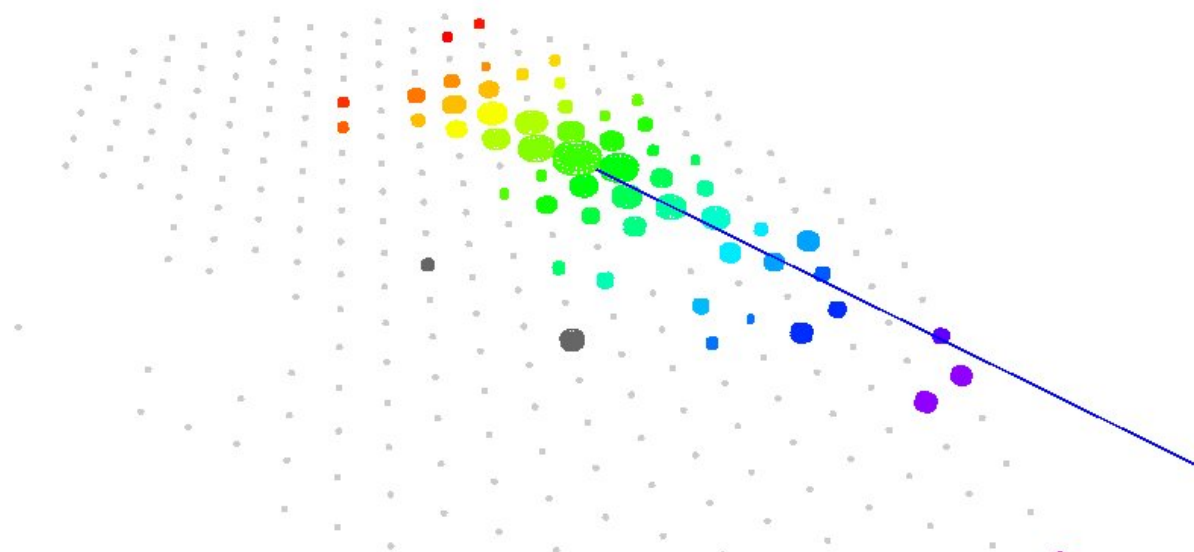
SD reconstruction



Beispiele sehr schräger Schauer




- 14.07.2008
- longest event: 65 km, 45 stations
- zenith: 87 degrees



- 17.08.2008
- highest multiplicity: 54 stations
- zenith: 82 degrees



An aerial photograph of a large, modern astronomical observatory building. The building features a prominent, wide, shallow, bowl-shaped roof made of corrugated metal panels, which is designed to house multiple telescopes. The central part of the building has a lower, more complex roof structure with a central opening. The building is situated in a desert environment with sparse vegetation. In the foreground, there are some construction materials and equipment, suggesting ongoing work or maintenance. The text "6 Telescope mit je 30x30 Grad Gesichtsfeld" is overlaid in yellow at the bottom of the image.

6 Telescope mit je 30x30 Grad Gesichtsfeld

Einzelnes Fluoreszenzteleskop

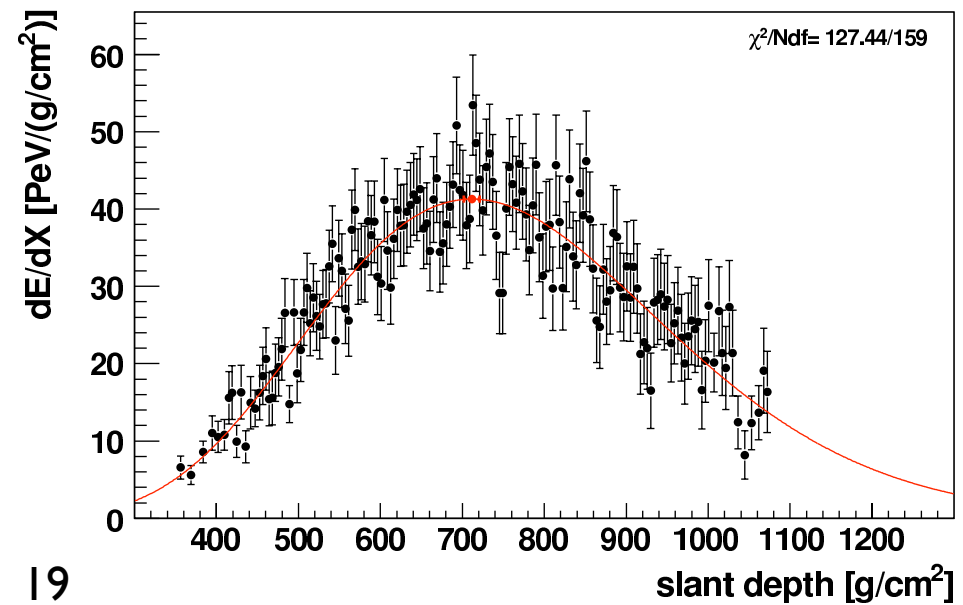
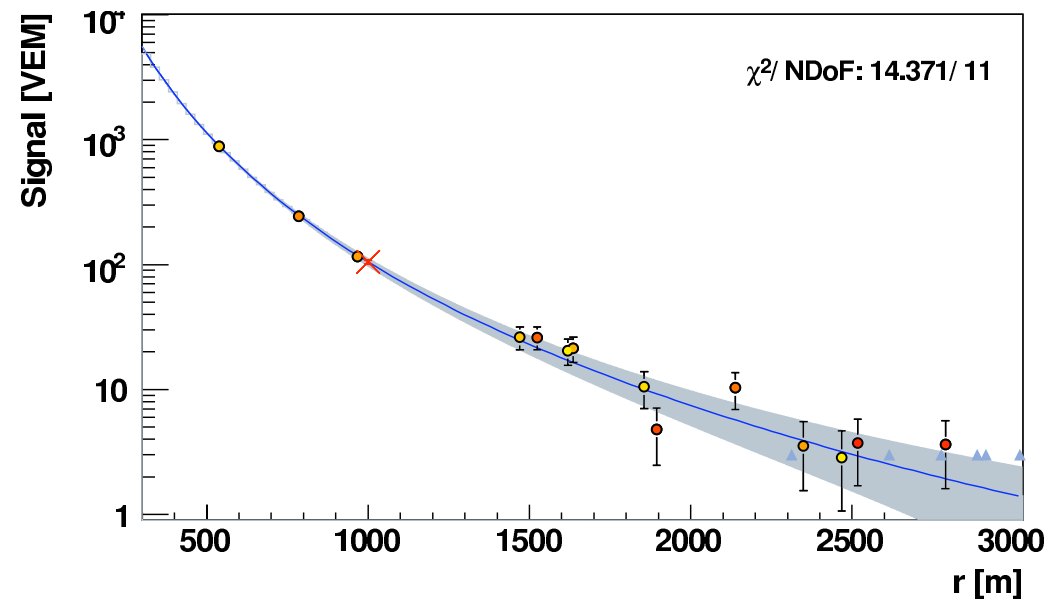
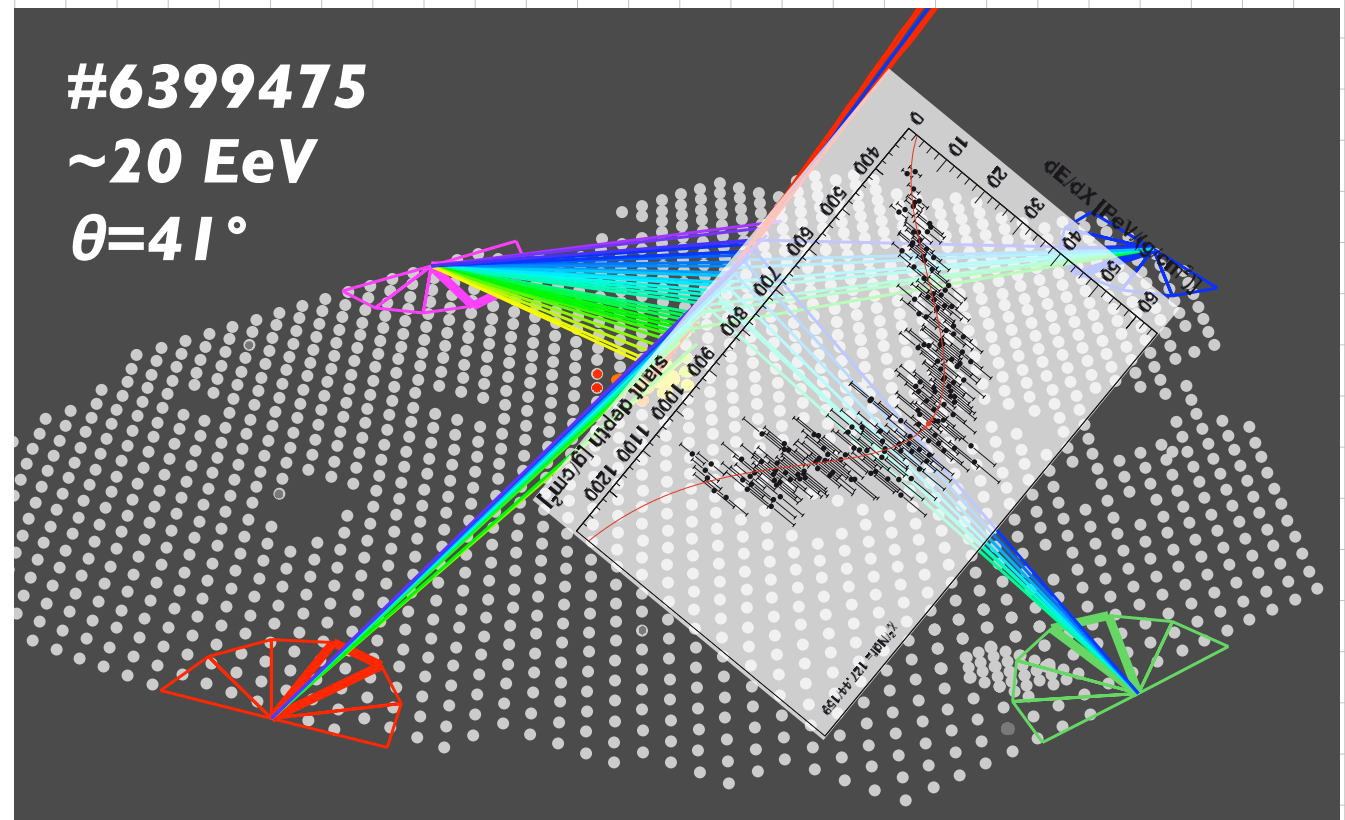
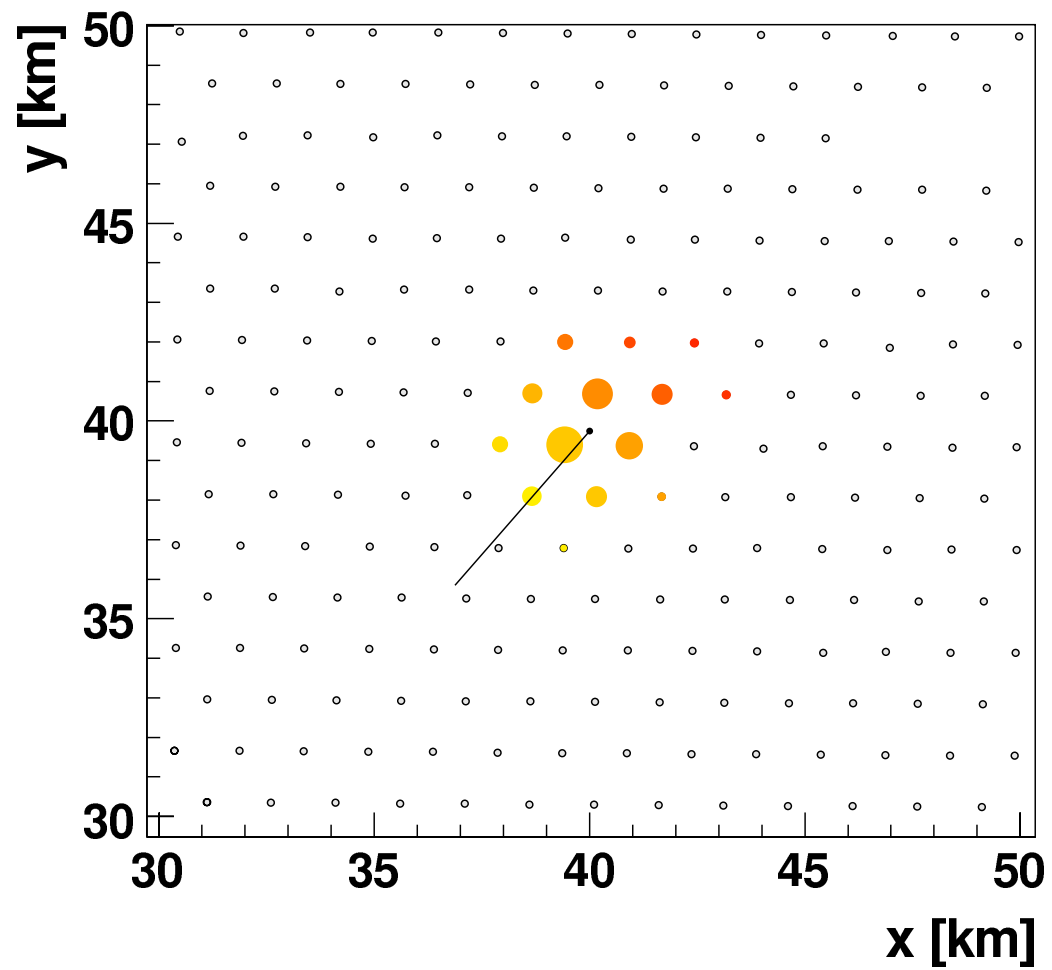


Kamera mit 440 Pixeln, aber 10
Millionen Bilder/Sekunde

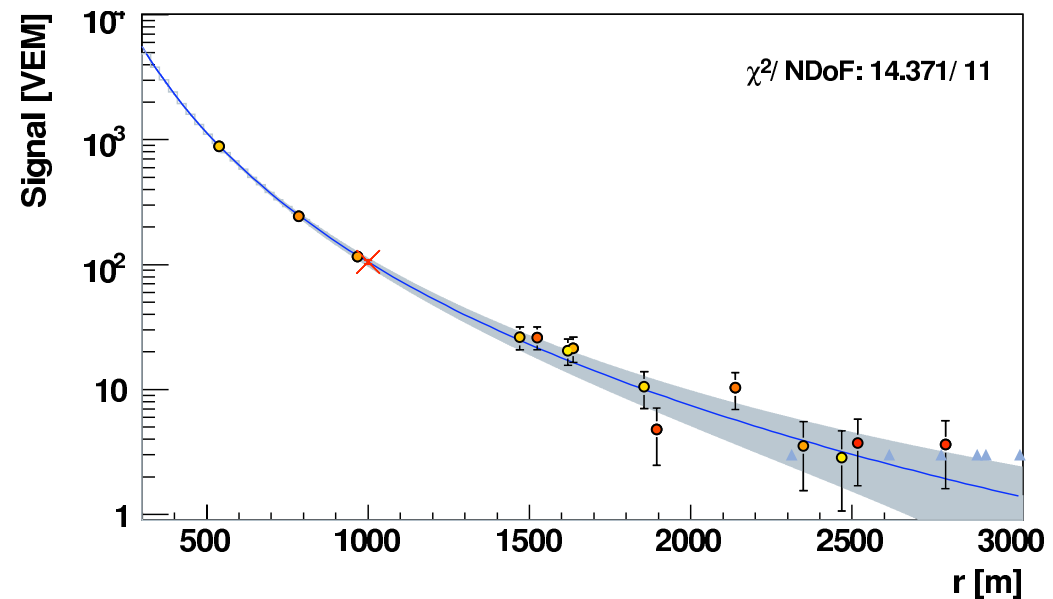
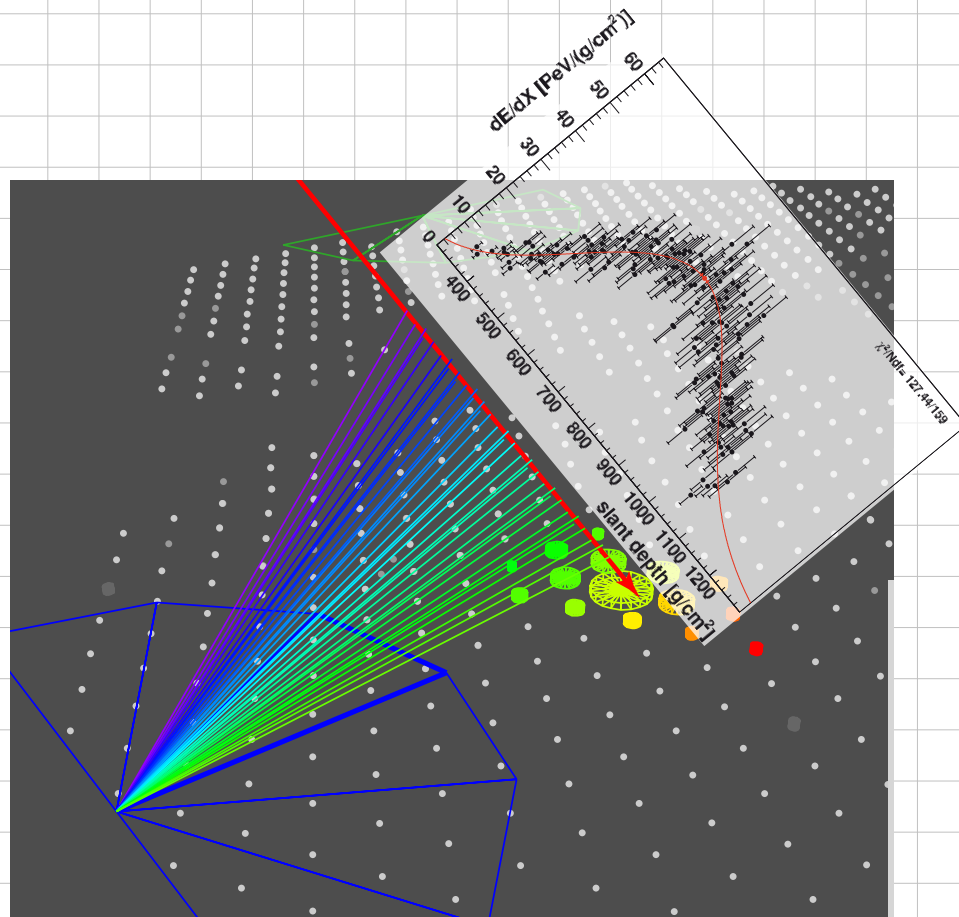
Apertur, UV-
durchlässiger
Filter und
Korrekturlinse

3.4 Meter
segmentierter
Spiegel

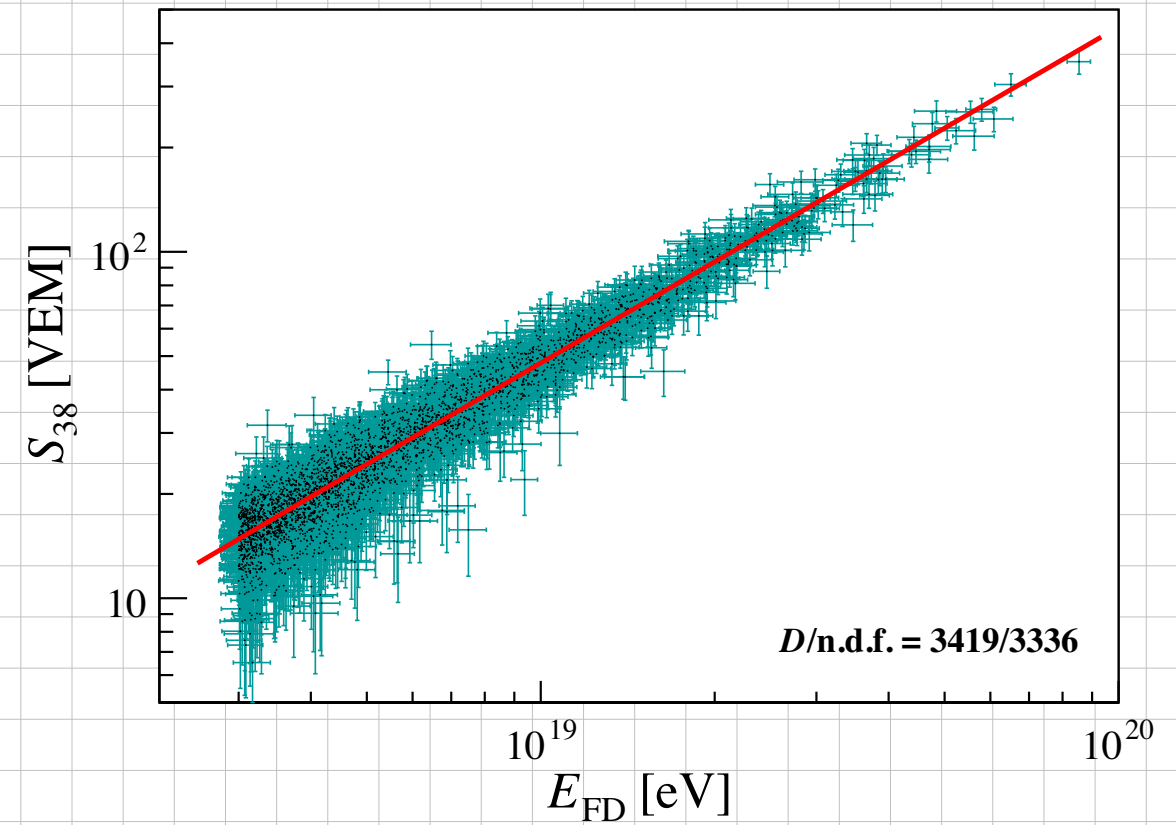
Hybrid-Messung



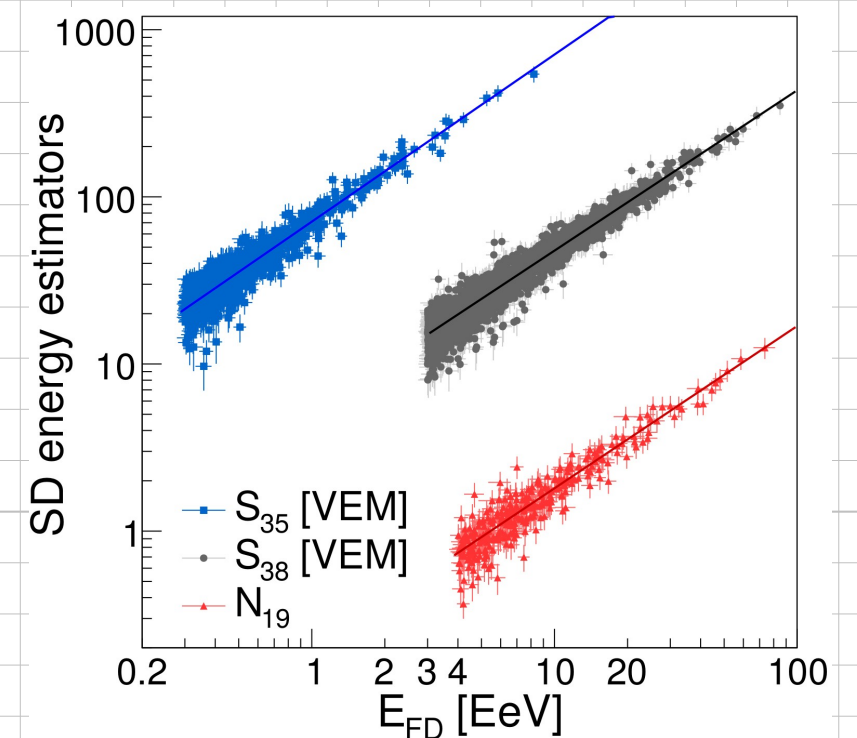
Energiekalibration des Oberflächendetektors



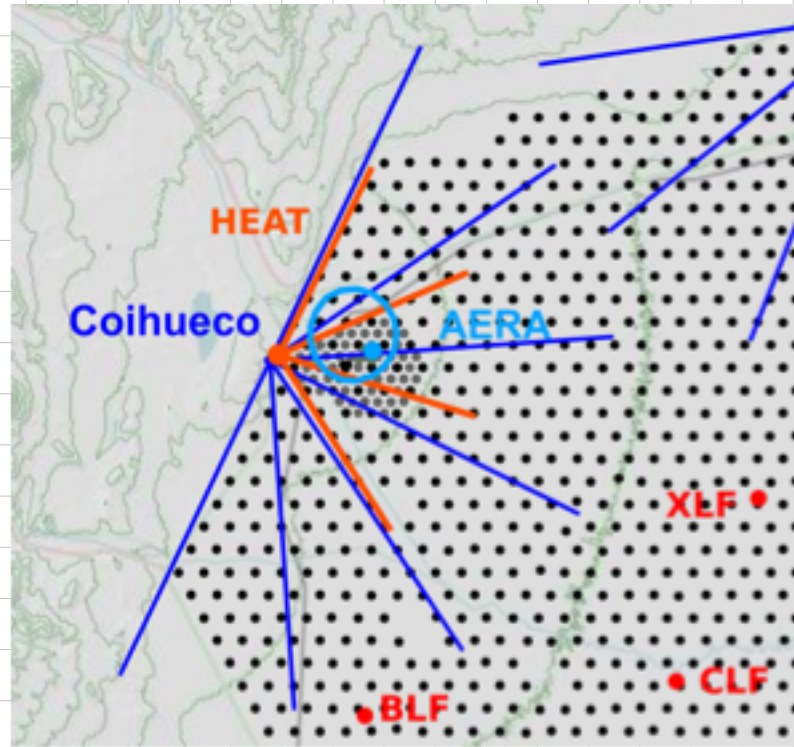
Oberflächensignal bei 1000m, $\theta=38^\circ$



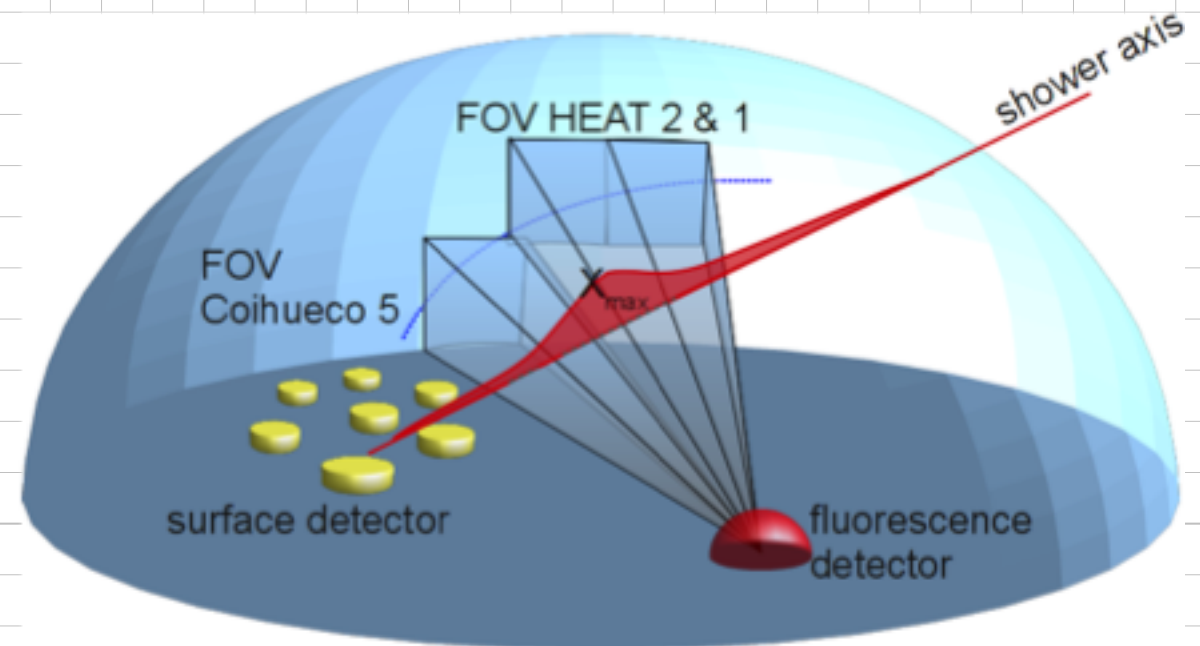
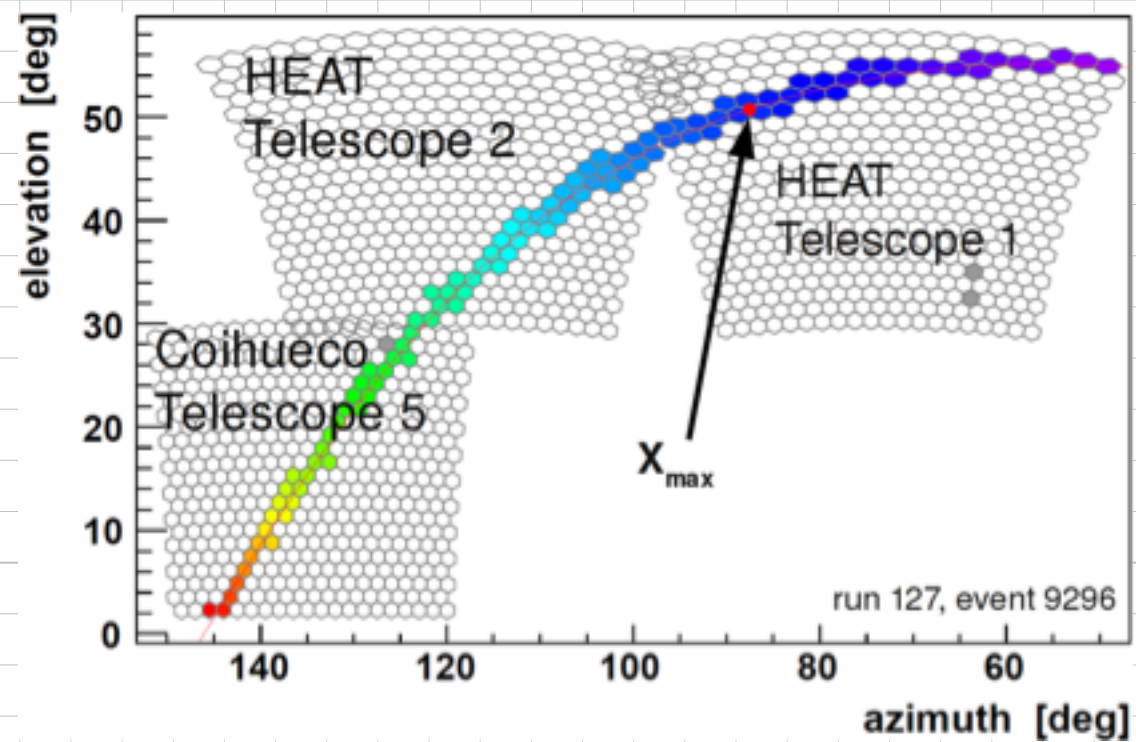
Energie gemessen mit
Fluoreszenzdetektor



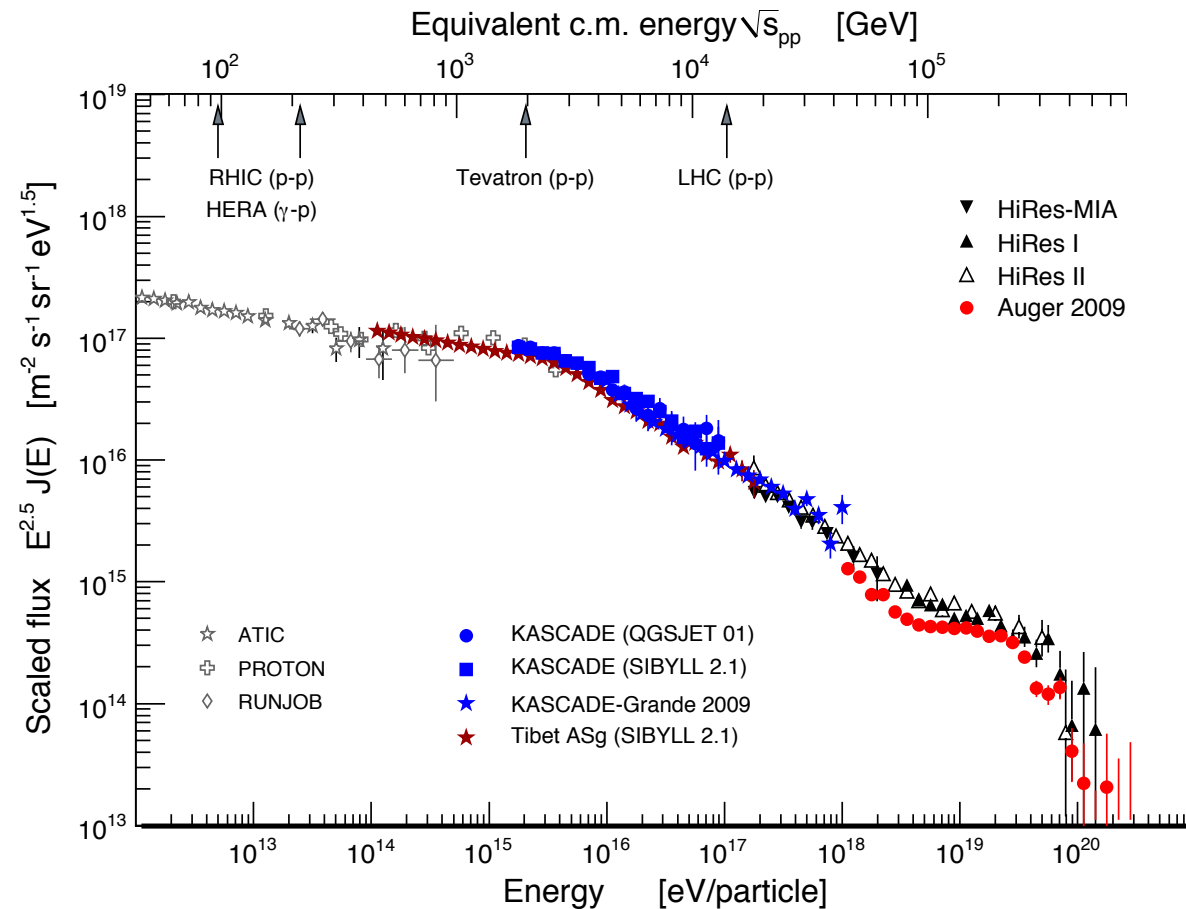
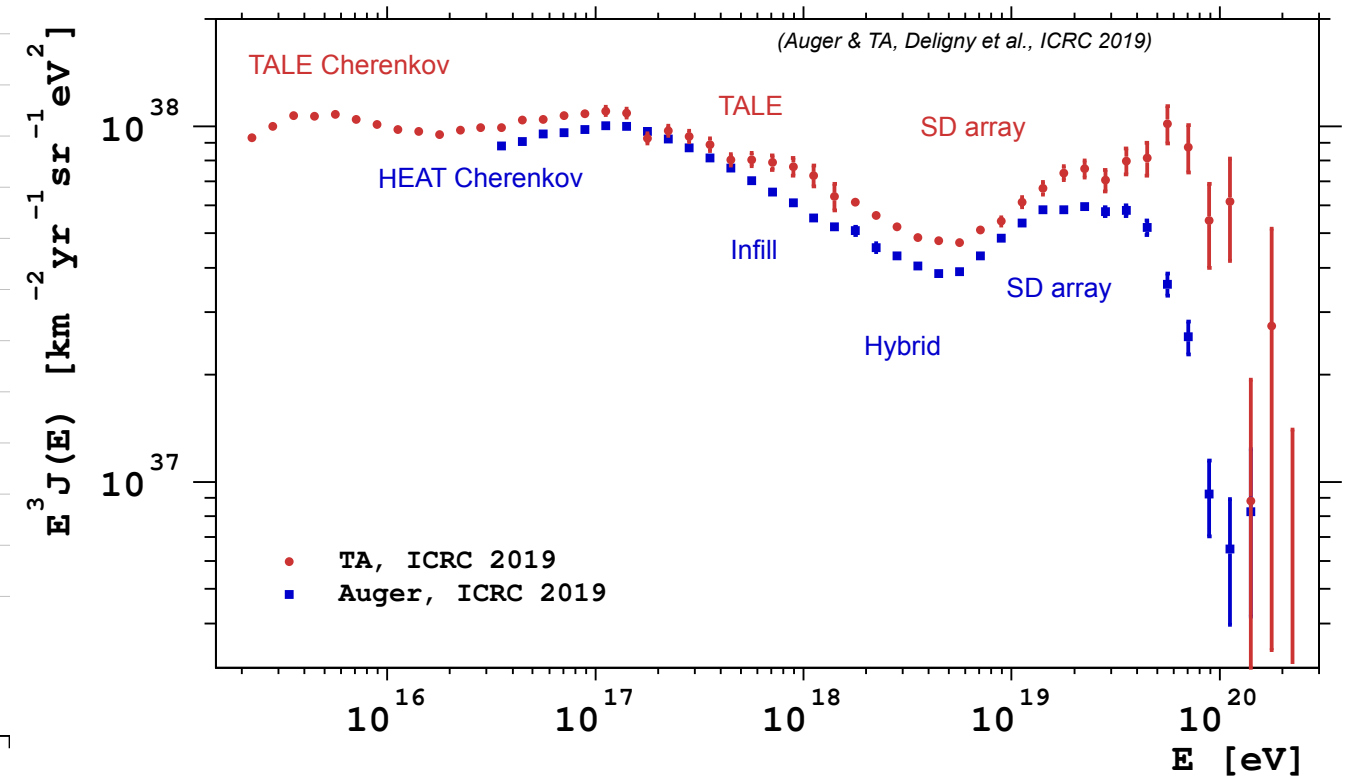
HEAT: FD+Cherenkov



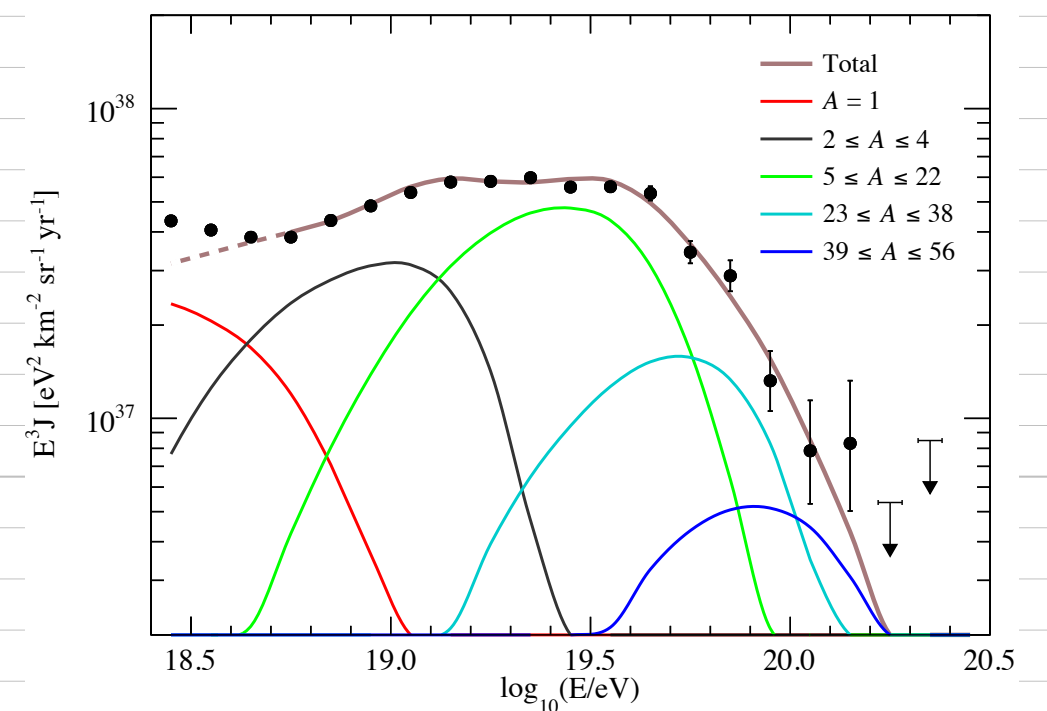
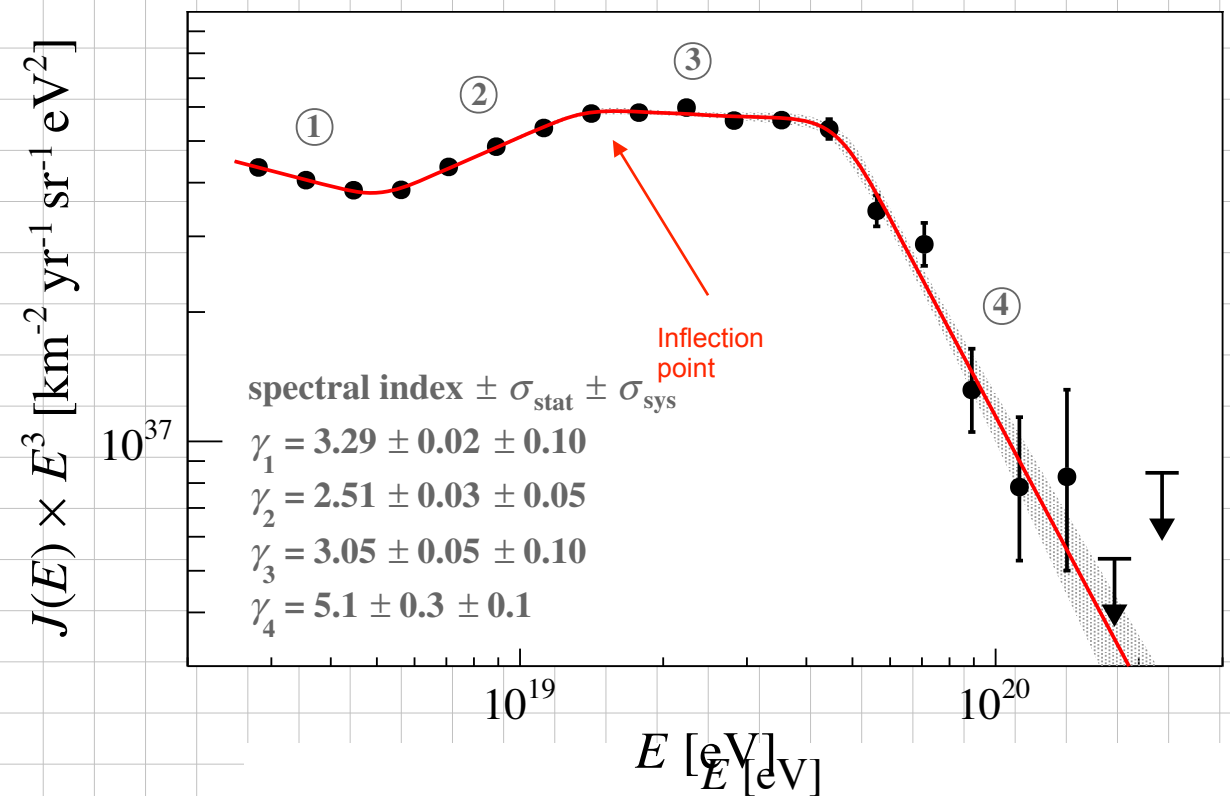
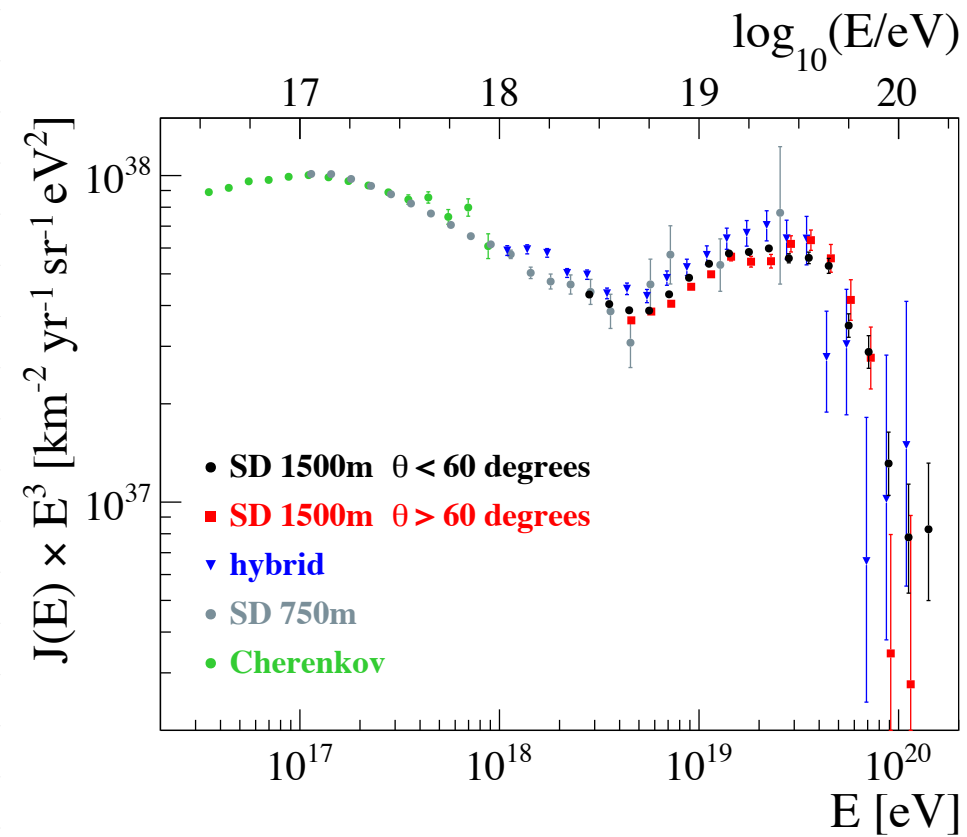
HEAT: High-Elevation Telescopes



Aktueller Stand der Flussmessungen

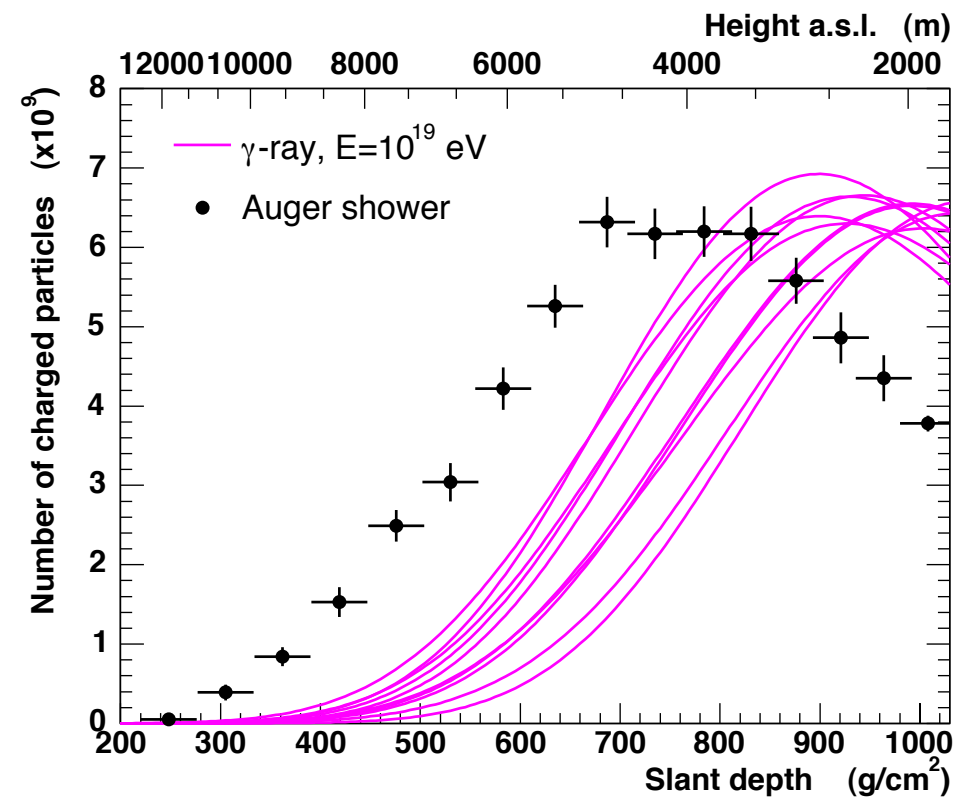
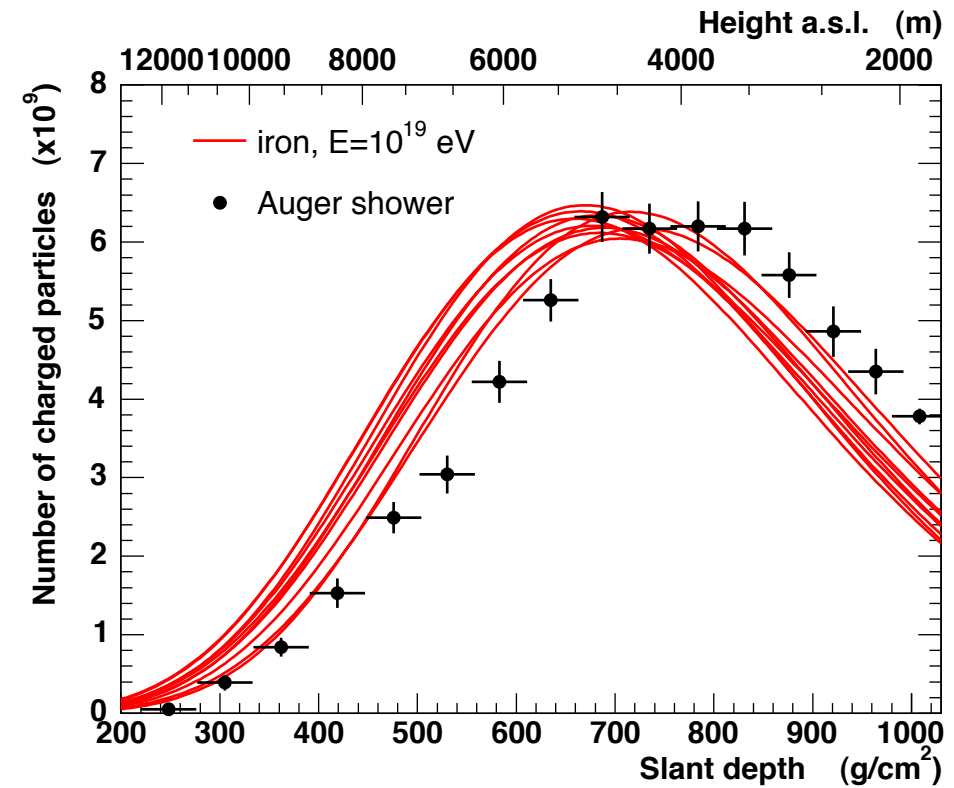
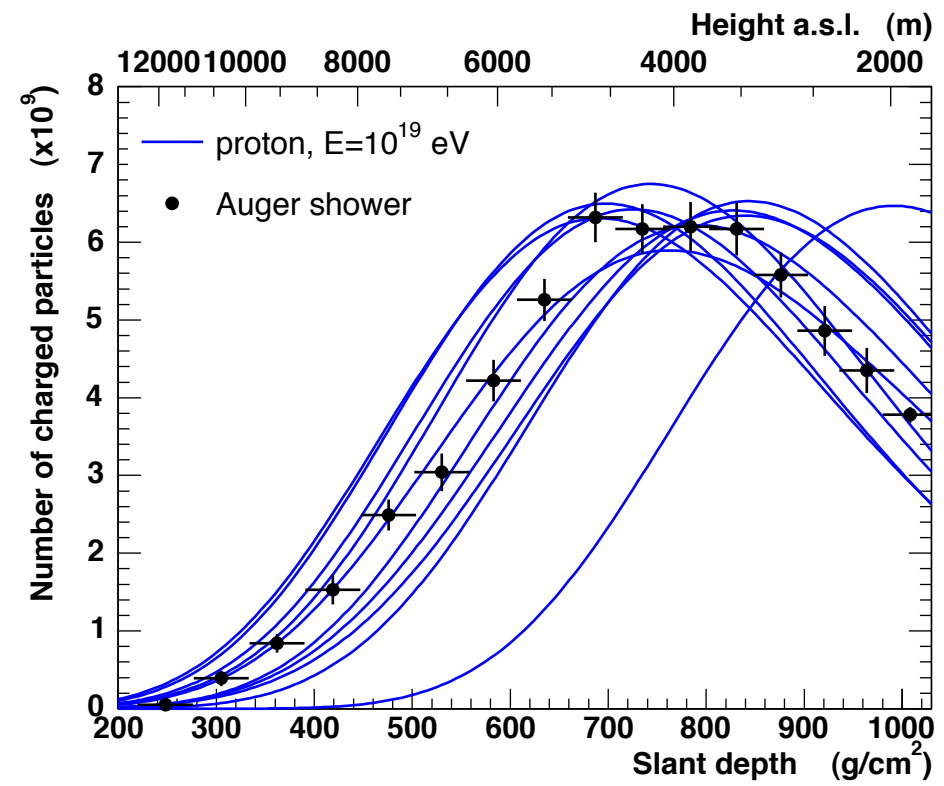


Resultate des Pierre-Auger-Observatoriums

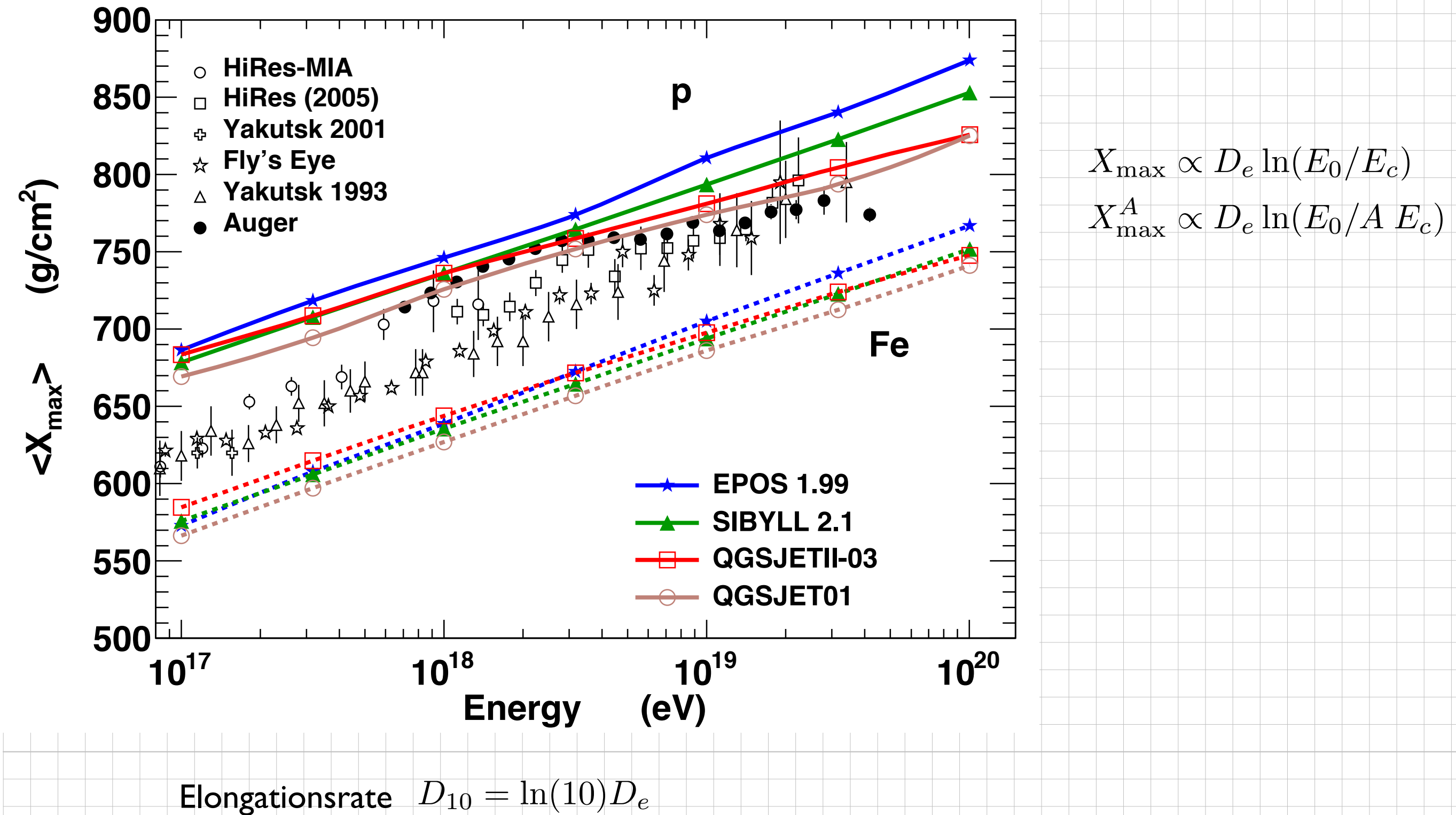


arXiv:1909.09073v1 [astro-ph.HE] 19 Sep 2019

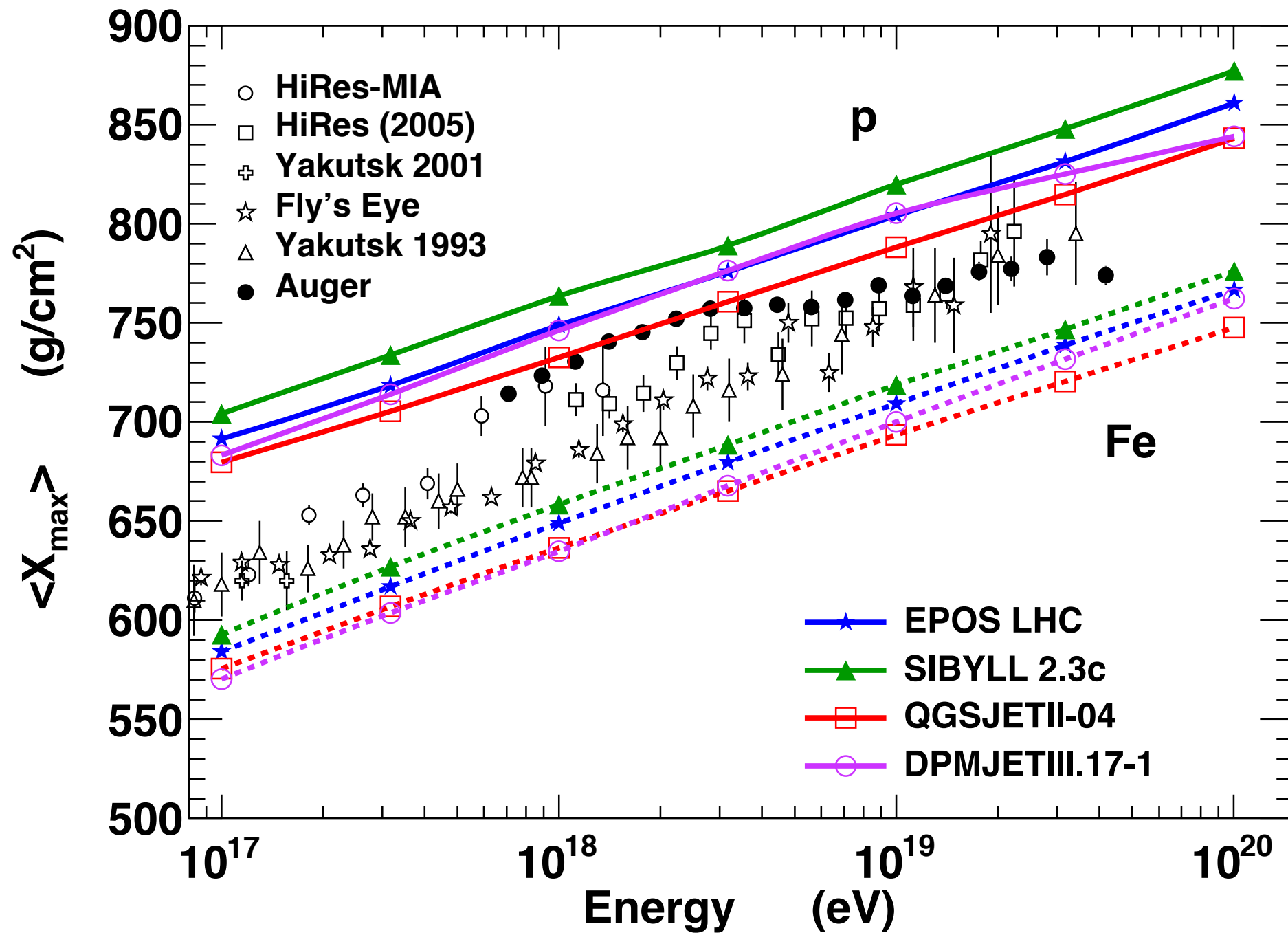
Primärteilchen: Longitudinale Schauerprofile



Mittlere Tiefe des Schauermaximums $\langle X_{\max} \rangle$



Mittlere Tiefe des Schauermaximums $\langle X_{\max} \rangle$

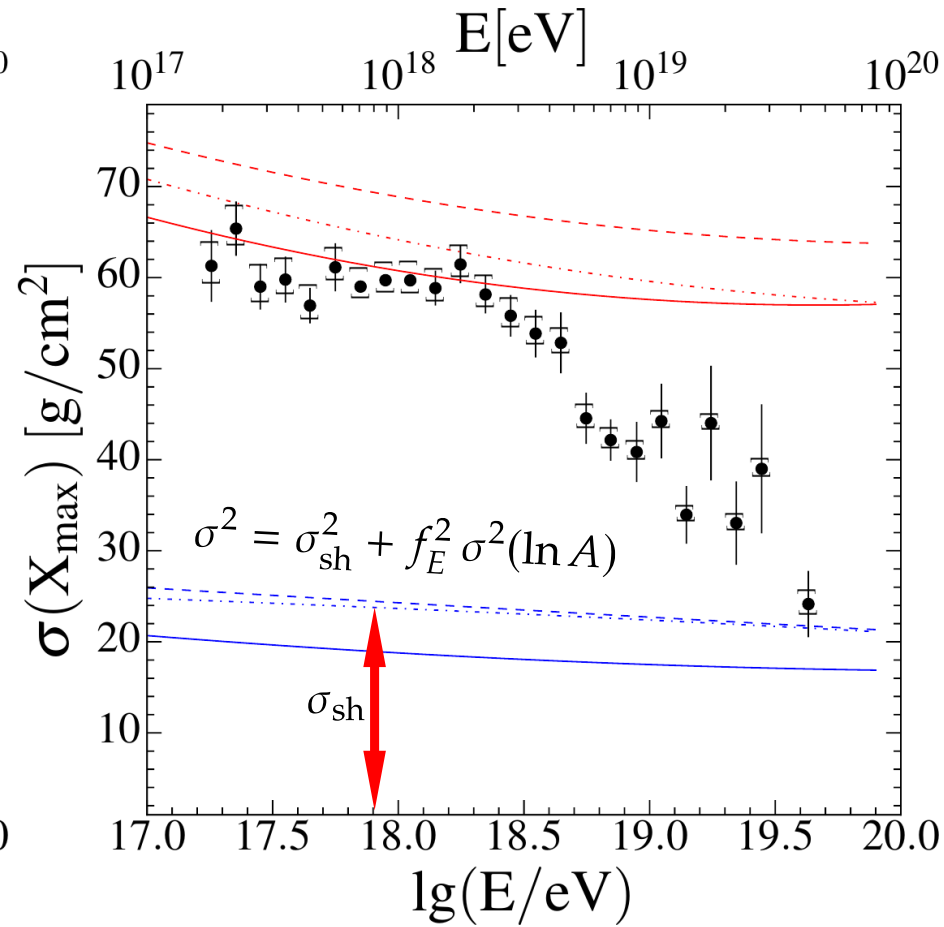
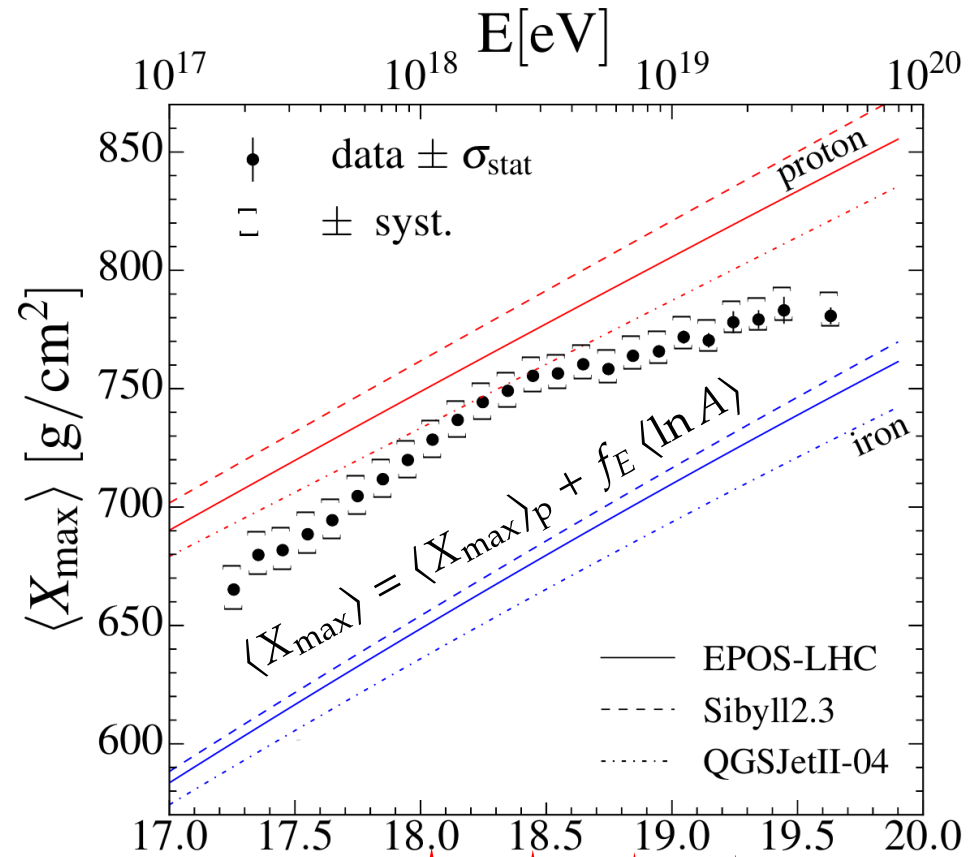


$$X_{\max} \propto D_e \ln(E_0/E_c)$$

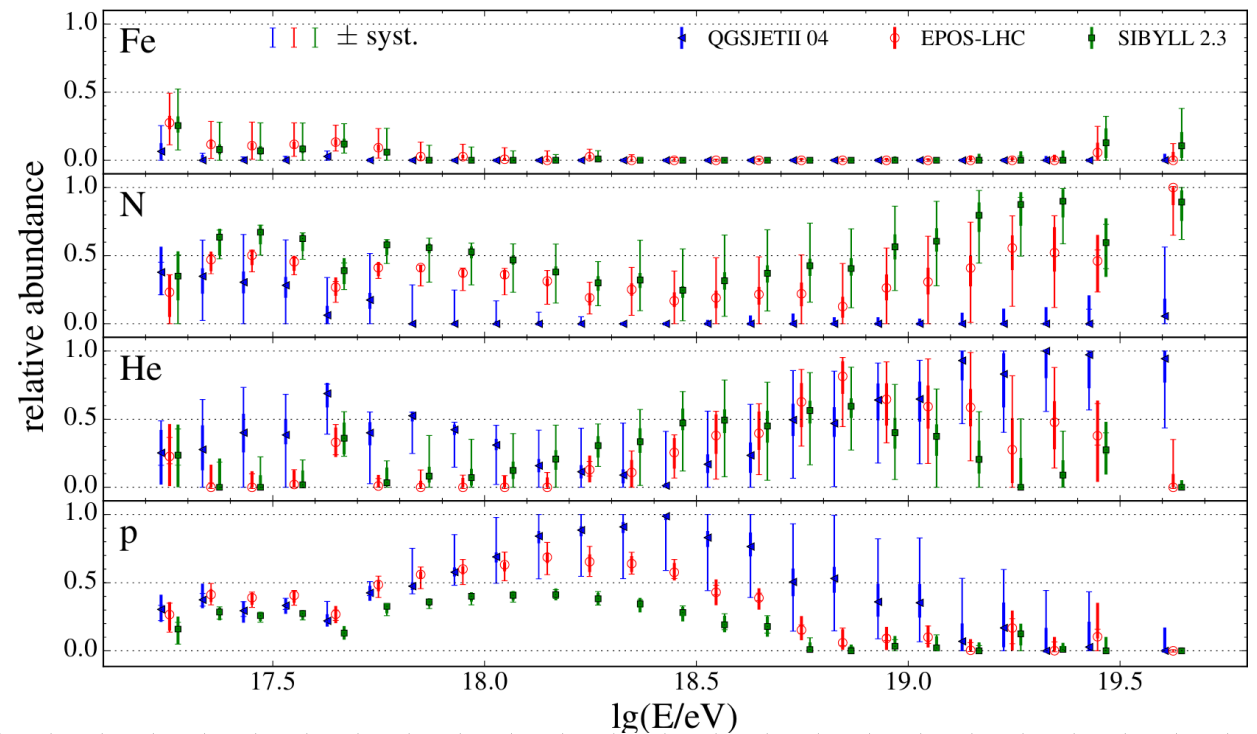
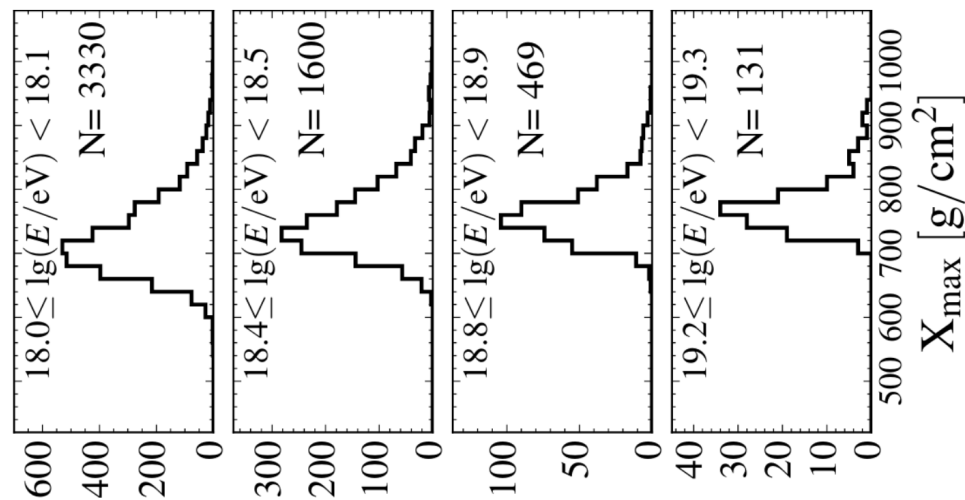
$$X_{\max}^A \propto D_e \ln(E_0/A E_c)$$

Elongationsrate $D_{10} = \ln(10) D_e$

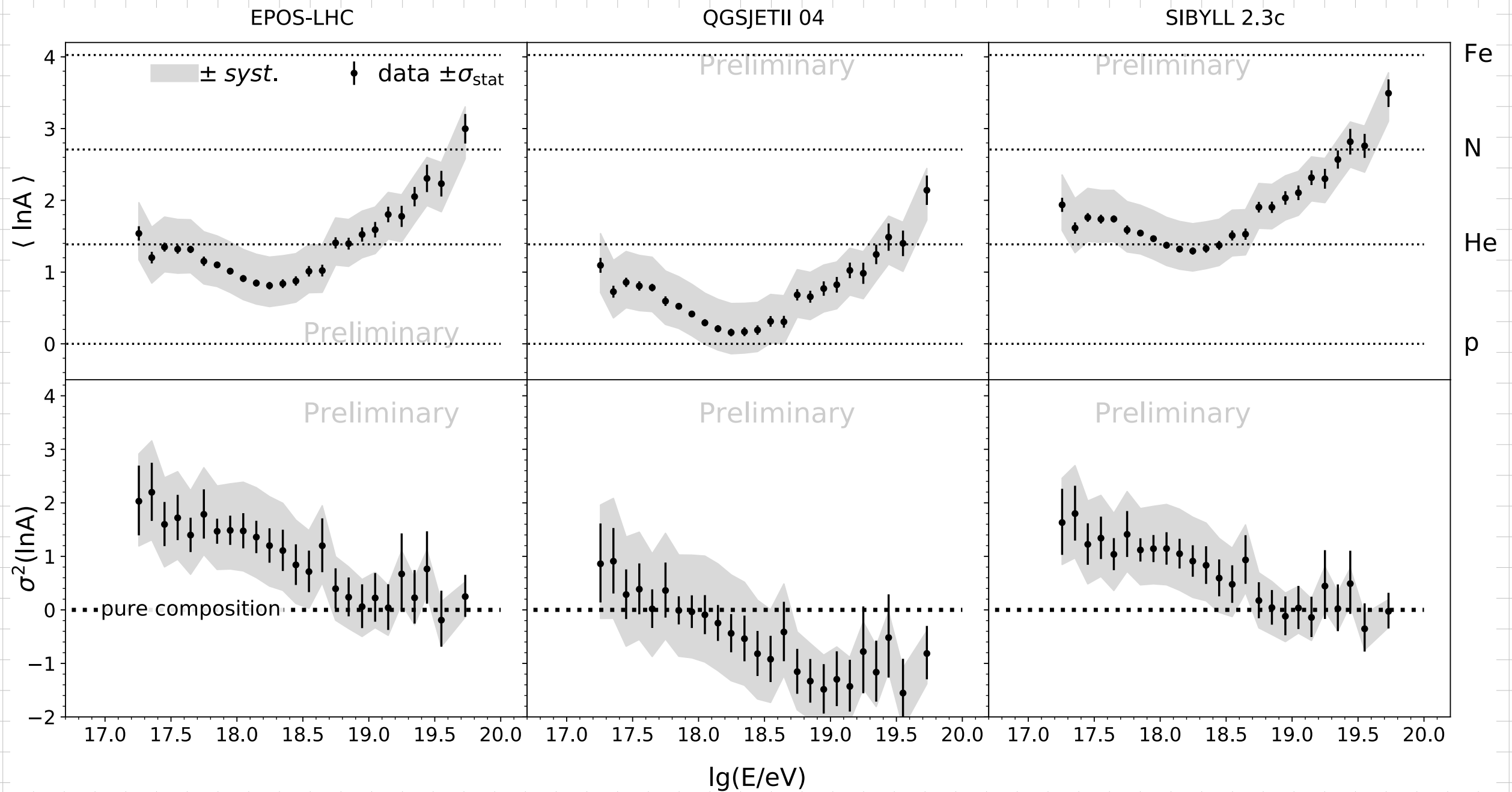
Depth of Shower Maxima



composition from X_{\max} distr. fits



Abhängigkeit von hadronischen Wechselwirkungsmodellen



Vorhersagen für das Schauermaximum

Kaskadentheorie: Schauermaximum für elektromagnetischen Schauer exakt bekannt

$$X_{\max} = X_0 \ln \left(\frac{E_0}{E_c} \right) \sim D_e^{\text{em}} \ln E_0$$

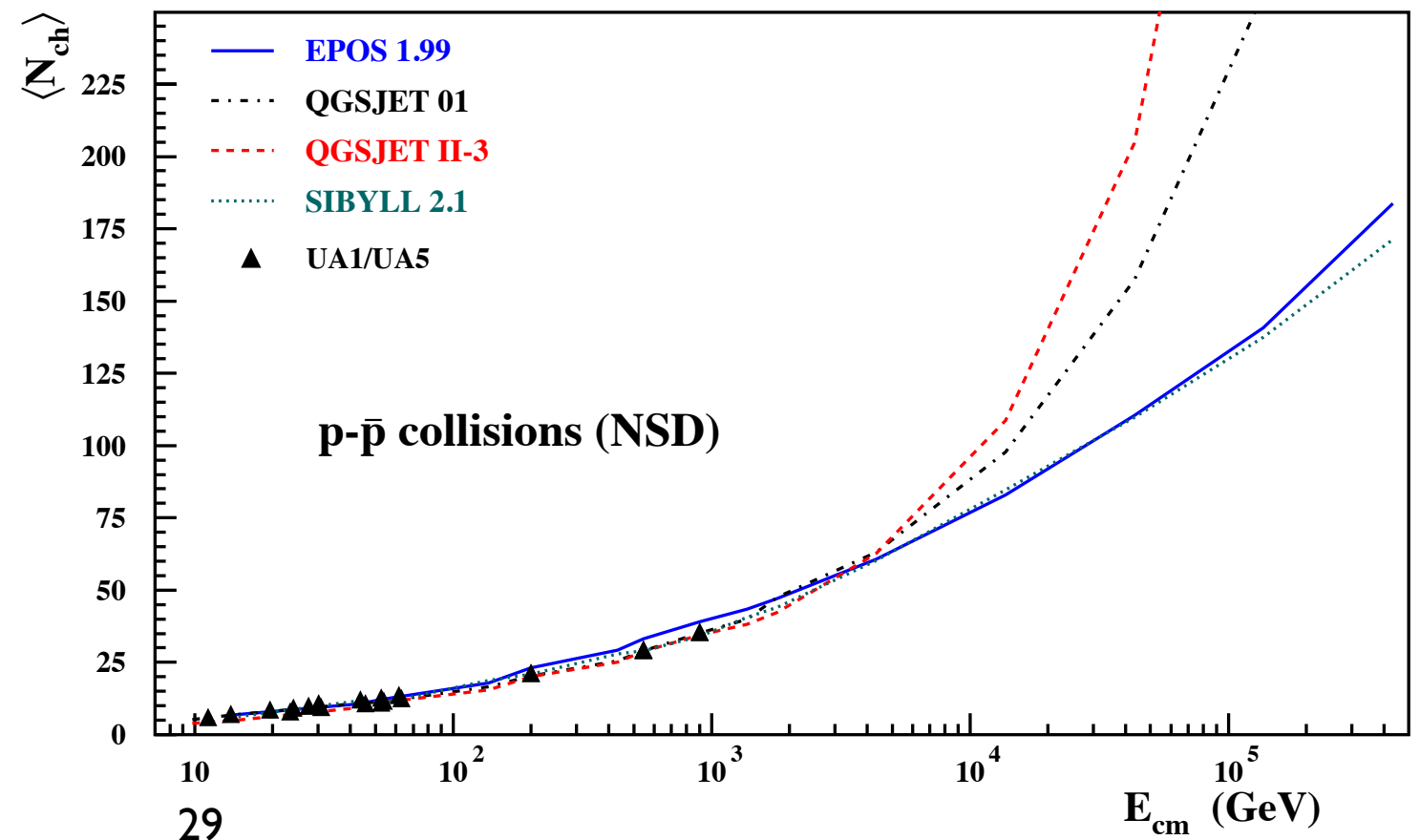
$$B_\lambda = -\frac{1}{X_0} \frac{d\lambda_{\text{int}}}{d \ln E}$$

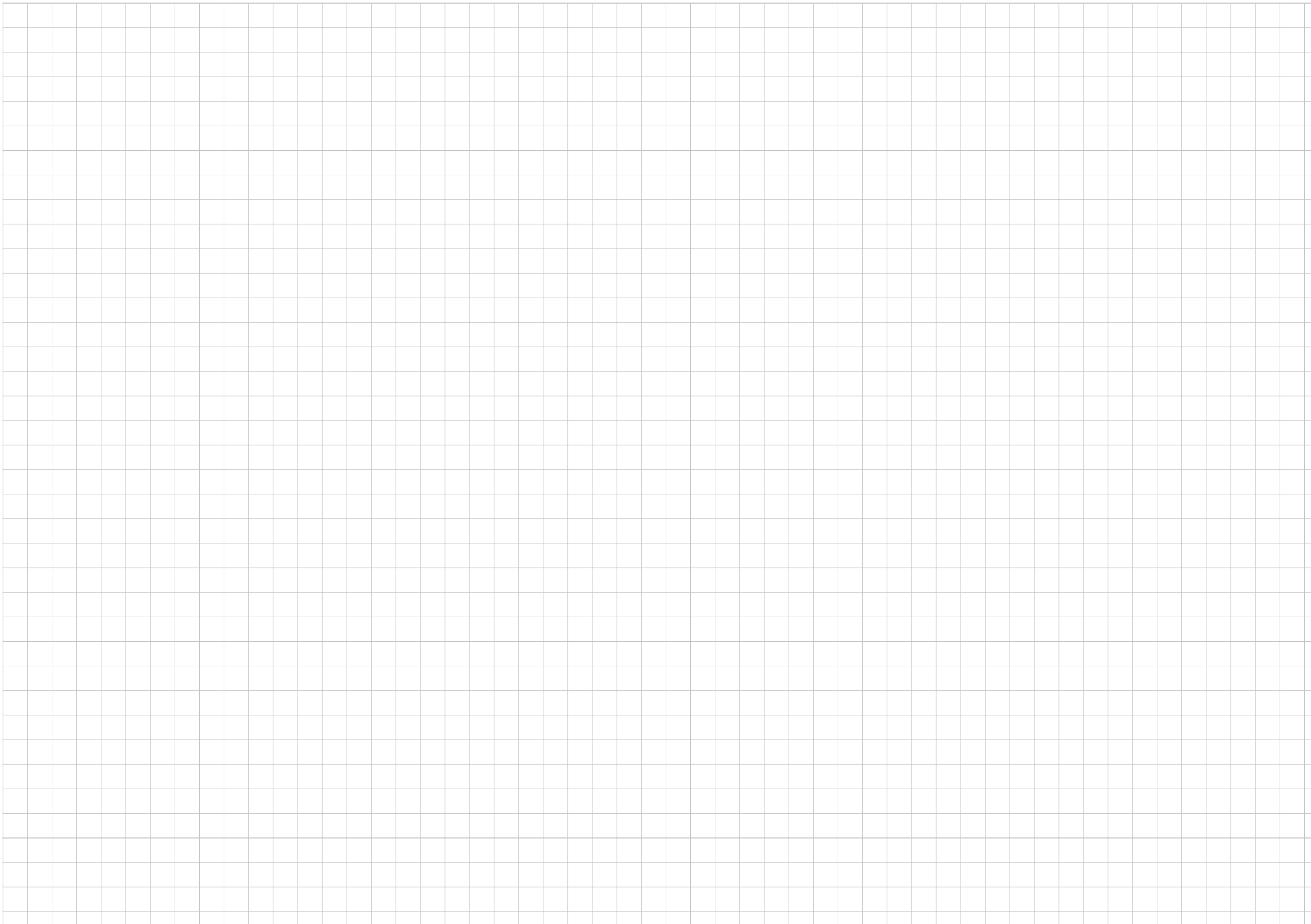
Elongationsratentheorem

(Linsley, Watson PRL46, 1981)

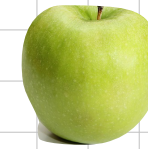
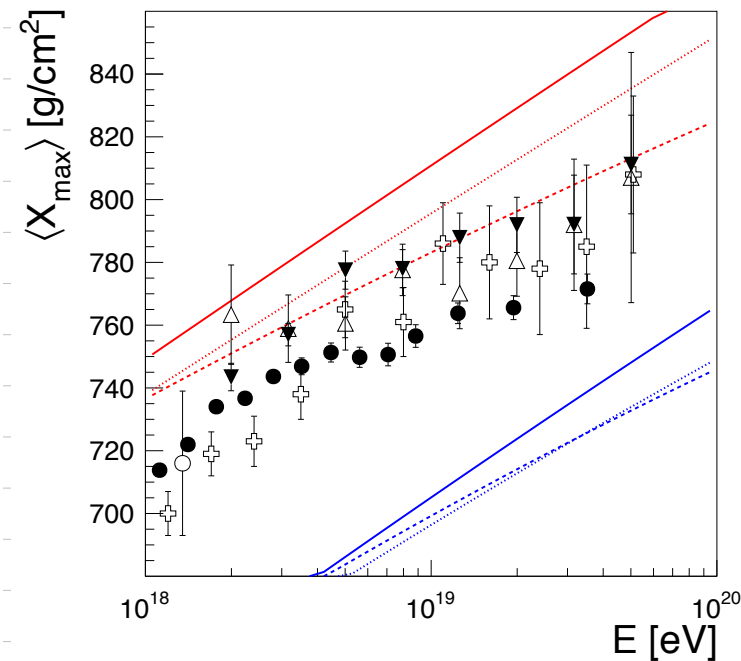
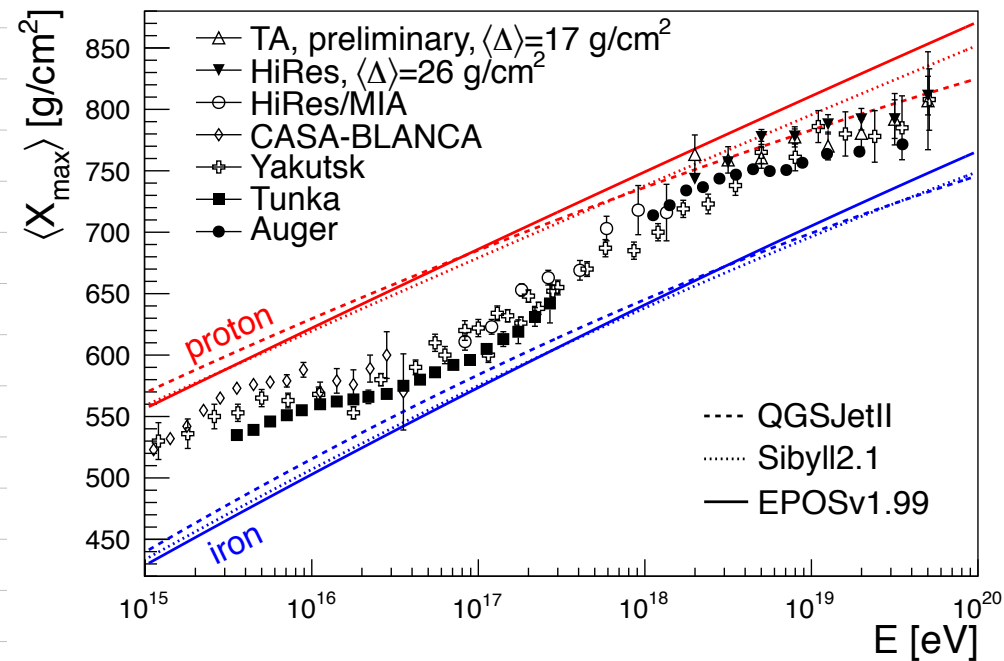
$$D_e^{\text{had}} = X_0(1 - B_\lambda - B_n)$$

$$B_n = \frac{d \ln n_{\text{tot}}}{d \ln E}$$



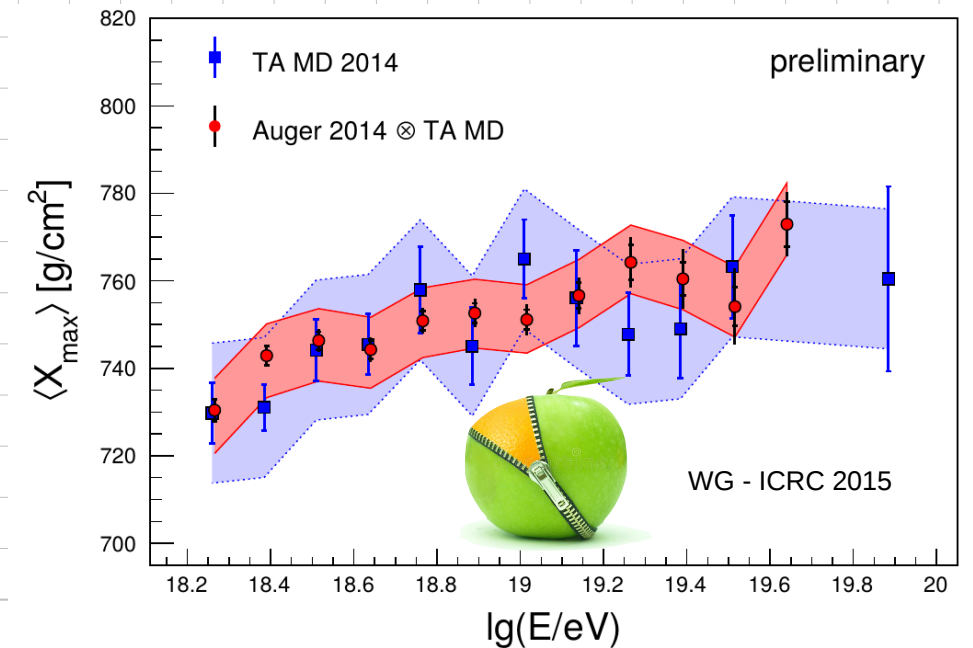
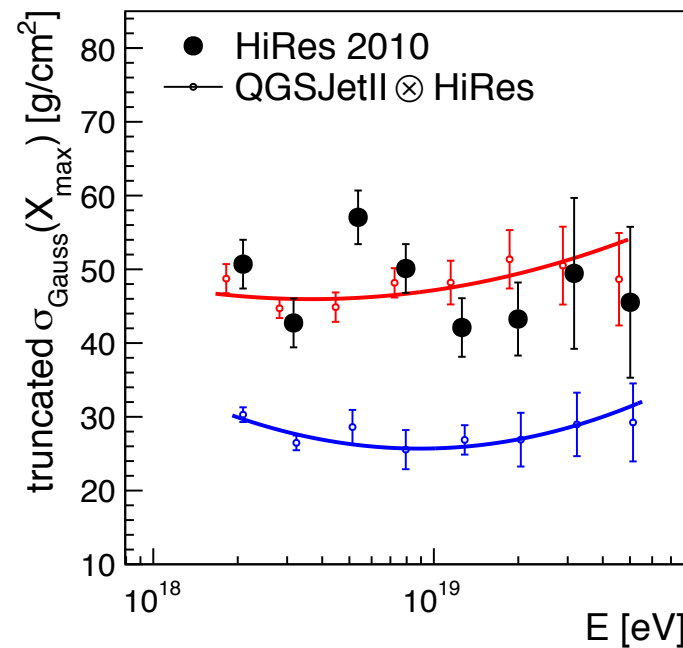
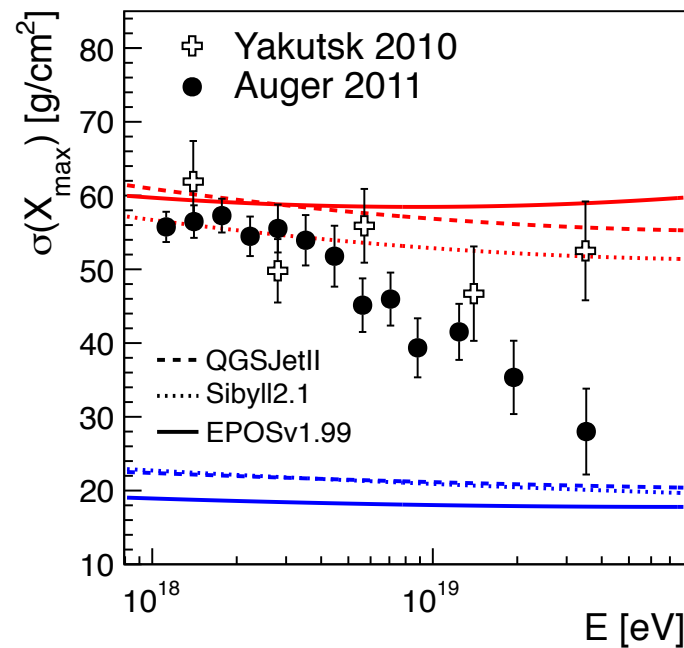


$\langle X_{\max} \rangle$ und Streuung



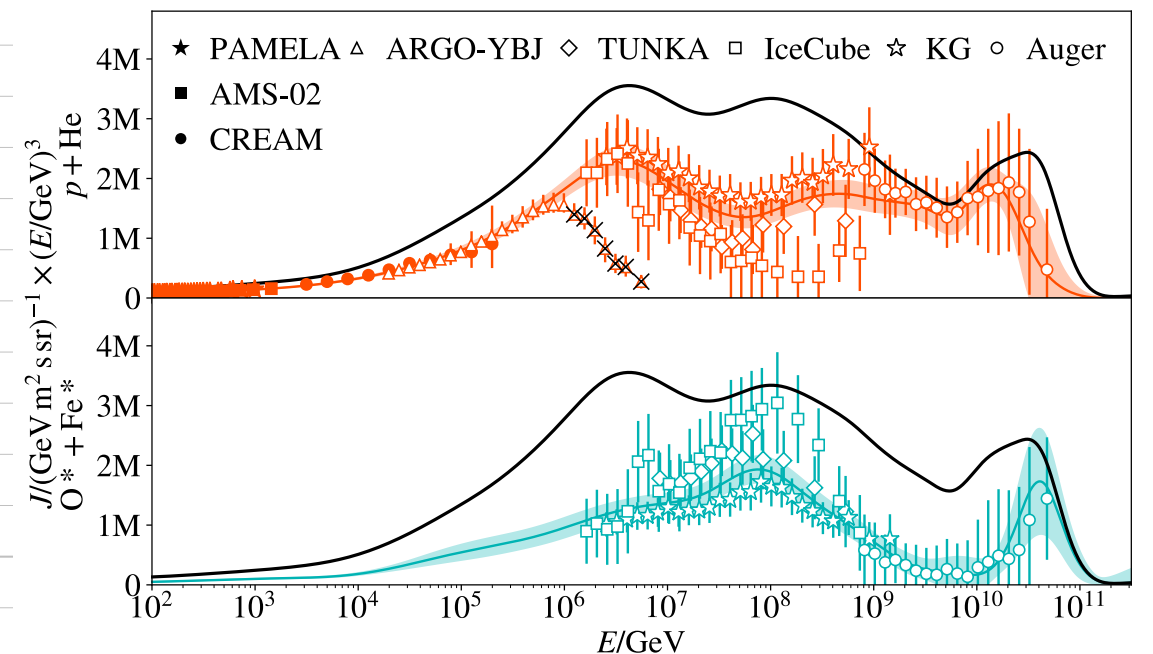
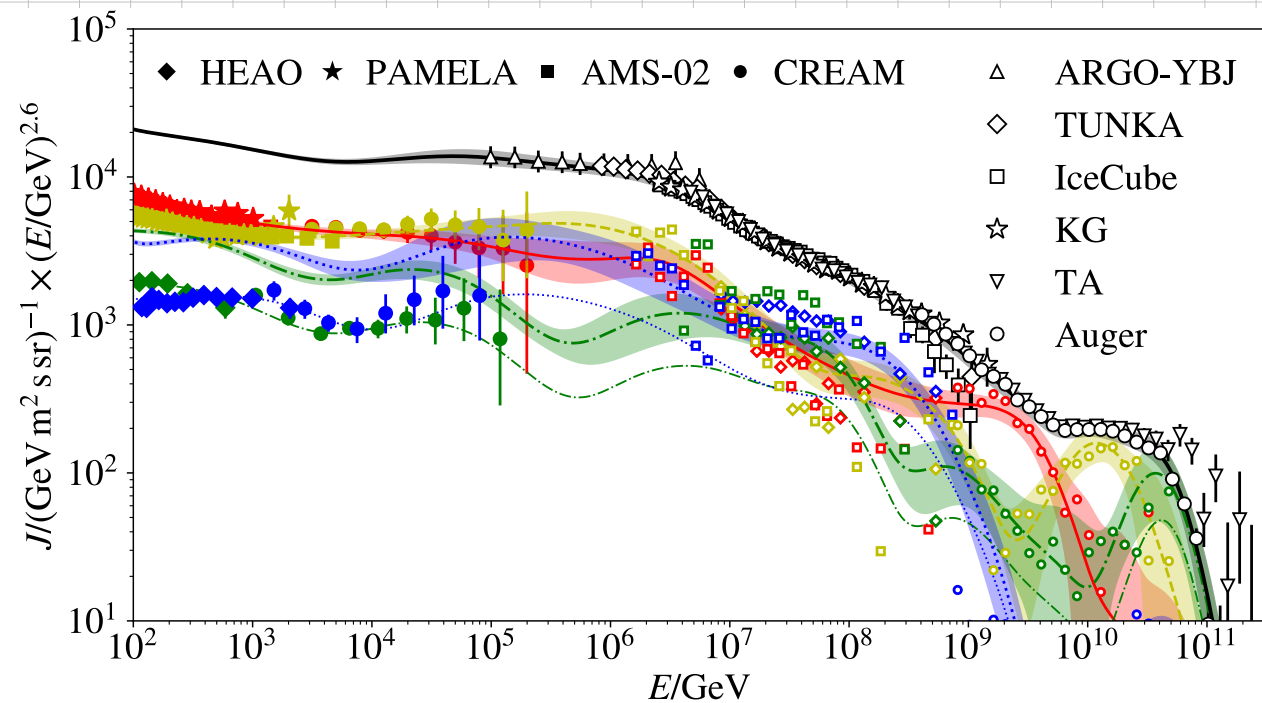
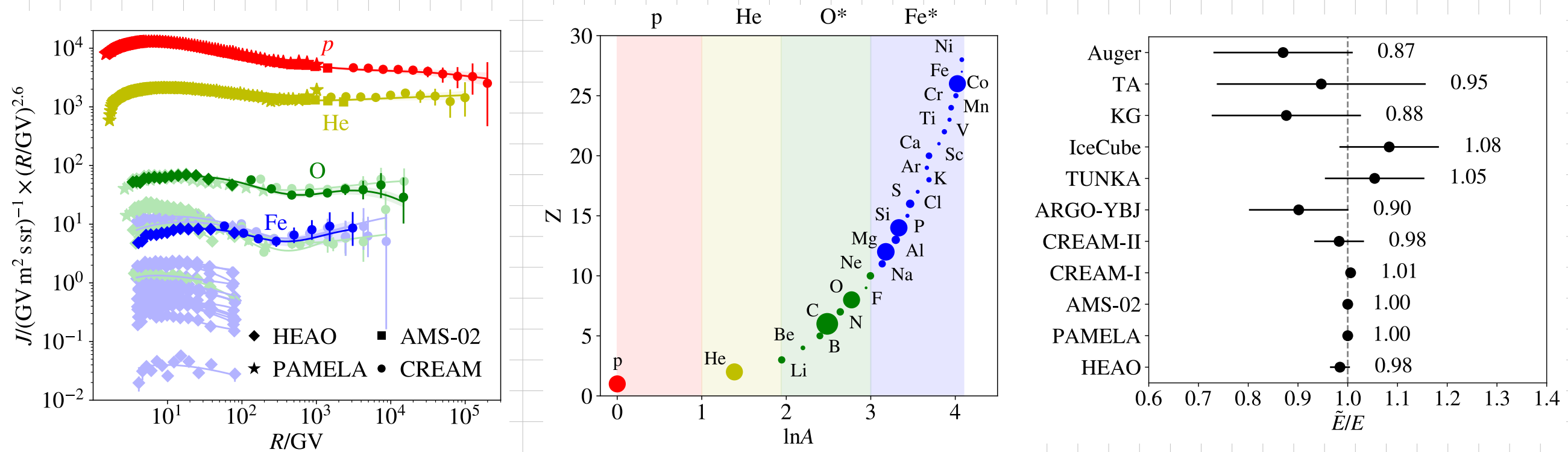
TA: all showers with X_{\max} in field of view
(bias due to detector acceptance)

Auger: only shower geometries for which all X_{\max} values visible



Unsicherheiten durch starke Modellabhängigkeit sehr groß

Phänomenologische Beschreibung: Energiespektrum und Elementzusammensetzung



Dipolstruktur (Auger)

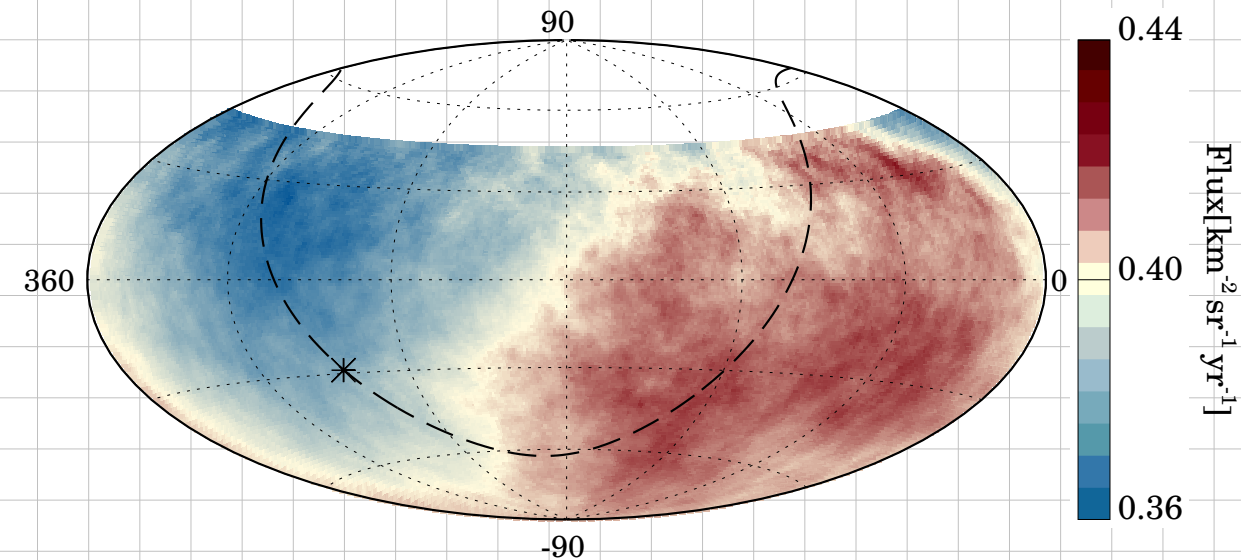


Figure 1: Map in Equatorial coordinates of the CR flux above 8 EeV, averaged on top-hat windows of 45° radius. The location of the Galactic plane is shown with a dashed line, and the Galactic center is indicated with a star.

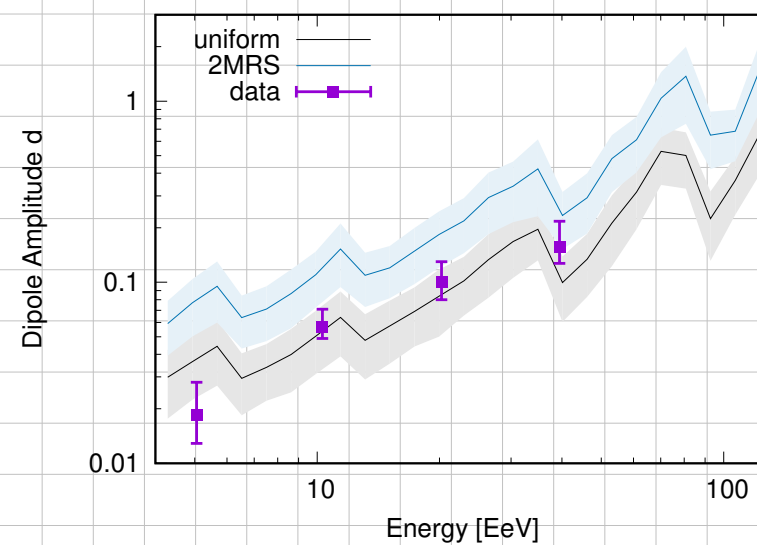


Figure 2: Energy dependence of the dipolar amplitude measured above 4 EeV. Also shown are the predictions from scenarios [12] with extragalactic sources.

Einfluss des galaktischen Magnetfelds auf einen Dipol

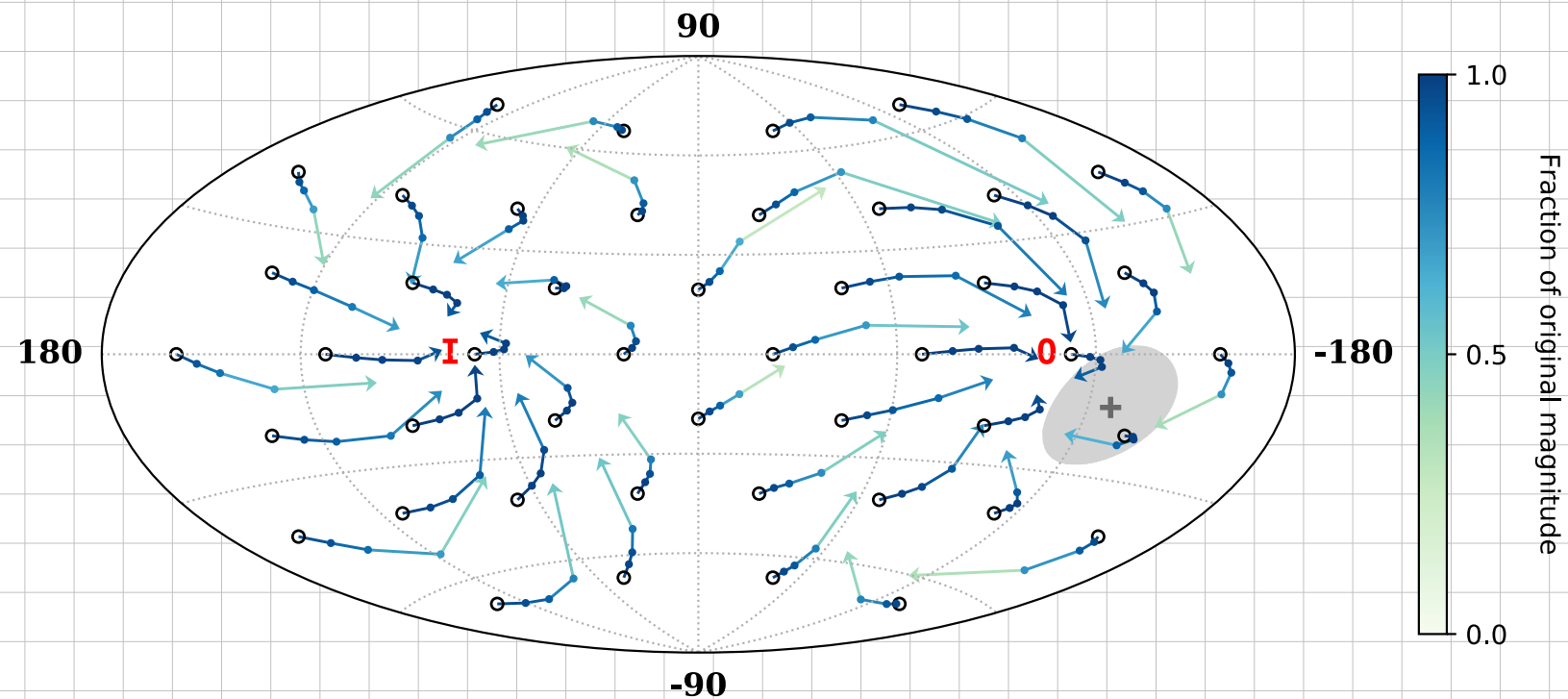


Figure 7. Change of the direction of the dipolar component of an extragalactic flux after traversing the Galactic magnetic field, modeled as in Jansson & Farrar (2012). We consider a grid (black circles) corresponding to the directions of a purely dipolar flux outside the Galaxy. Points along the lines indicate the reconstructed directions for different values of the particle rigidity: 32, 16, and 8 EV, and, at the tip of the arrow, 4 EV. The line color indicates the resulting fractional change of the dipole amplitude. The observed direction of the dipole for energies $E \geq 8$ EeV is indicated by the gray plus sign, with the shaded area indicating the 68% CL region. The labels *I* and *O* indicate the directions toward the inner and outer spiral arms, respectively.

Dipolentwicklung mit Energie

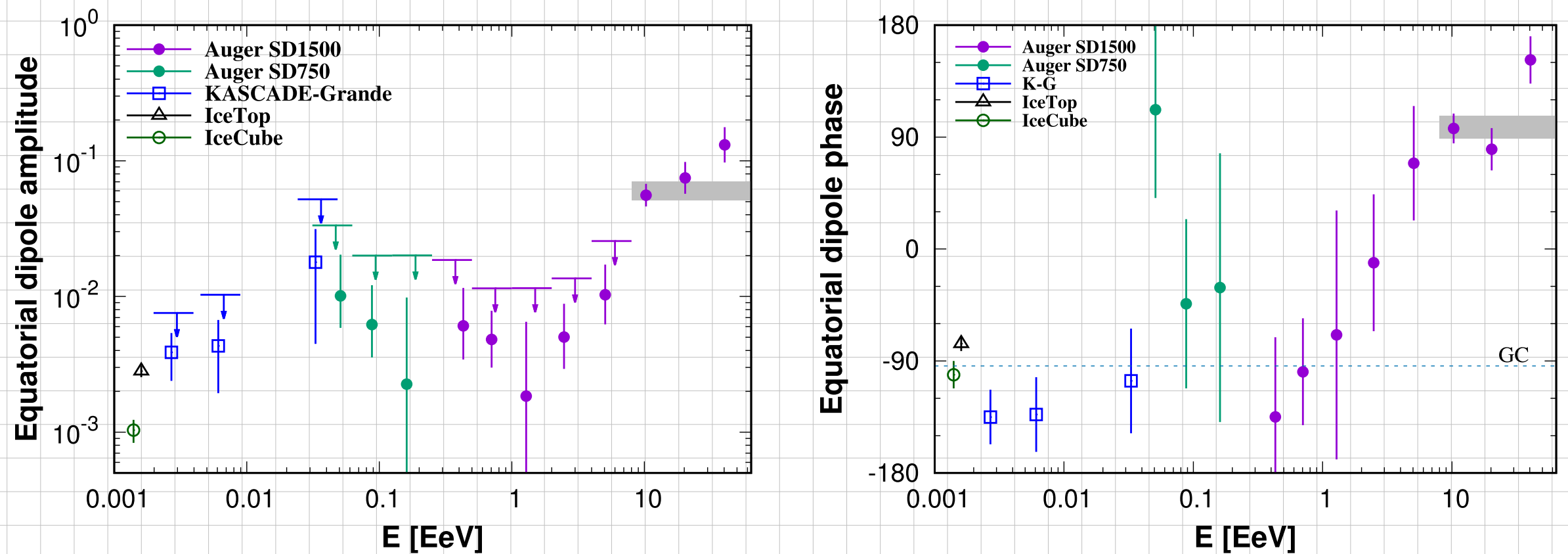
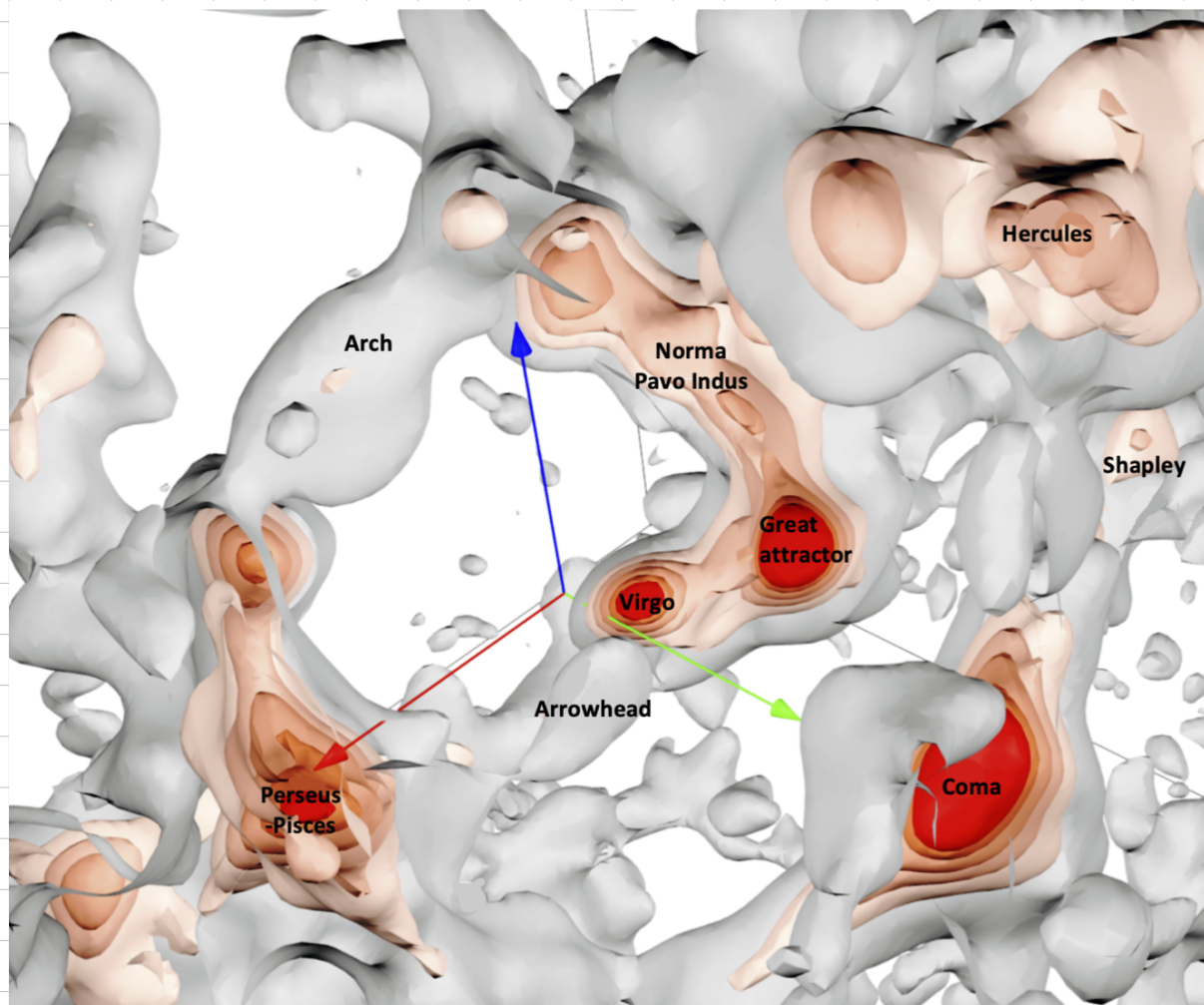
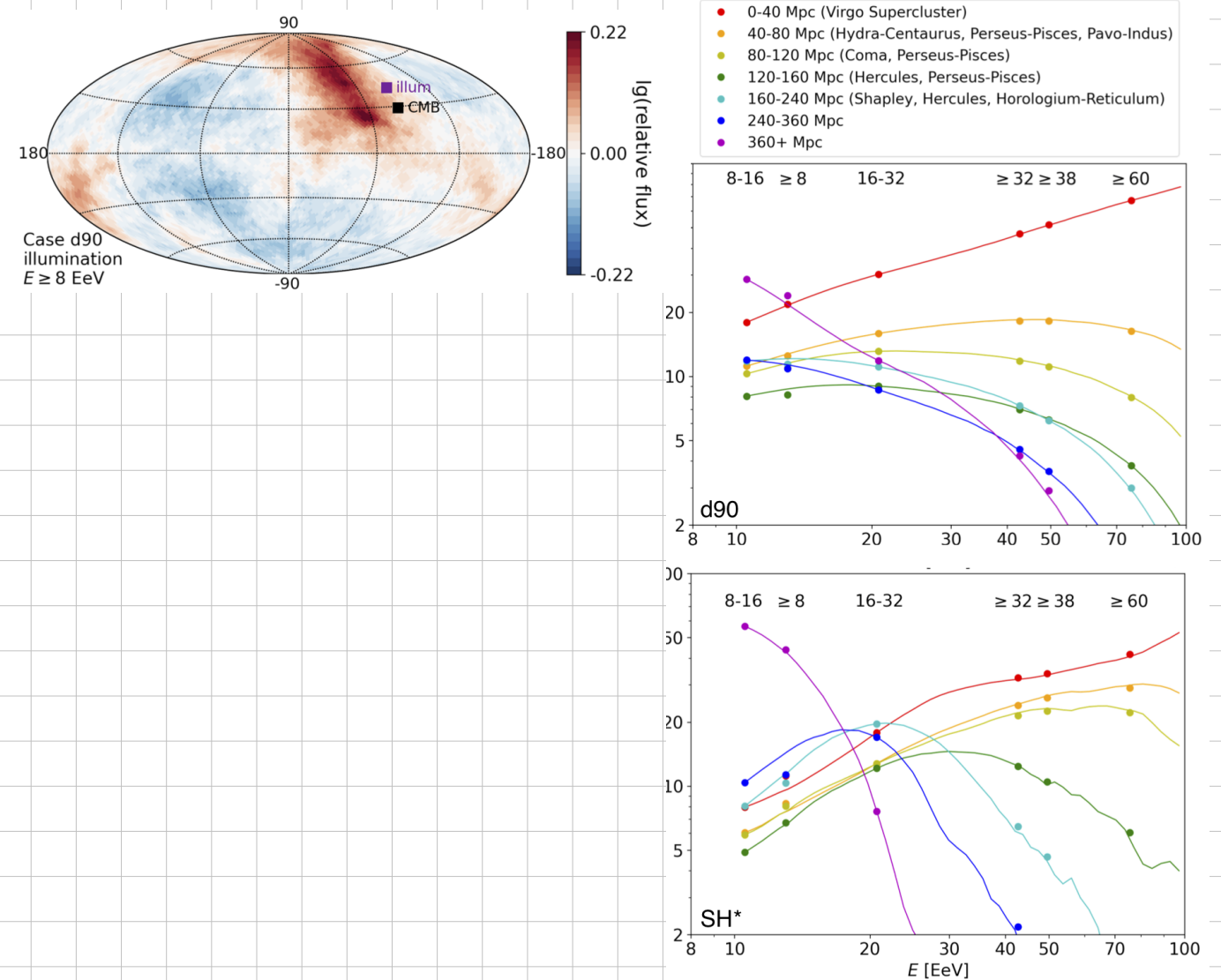


Figure 1. Reconstructed equatorial dipole amplitude (left) and phase (right). The upper limits at 99% CL are shown for all the energy bins in which the measured amplitude has a chance probability greater than 1%. The gray bands indicate the amplitude and phase for the energy bin $E \geq 8$ EeV. Results from other experiments are shown for comparison (IceCube Collaboration 2012, 2016; KASCADE-Grande Collaboration 2019).

The Imprint of Large Scale Structure on the Ultra-High-Energy Cosmic Ray Sky



[<https://sketchfab.com/3d-models/quasi-linear-construction-of-the-density-field-91448f58ed5b4a30b5dc270a34fb4352>]



The Imprint of Large Scale Structure on the Ultra-High-Energy Cosmic Ray Sky

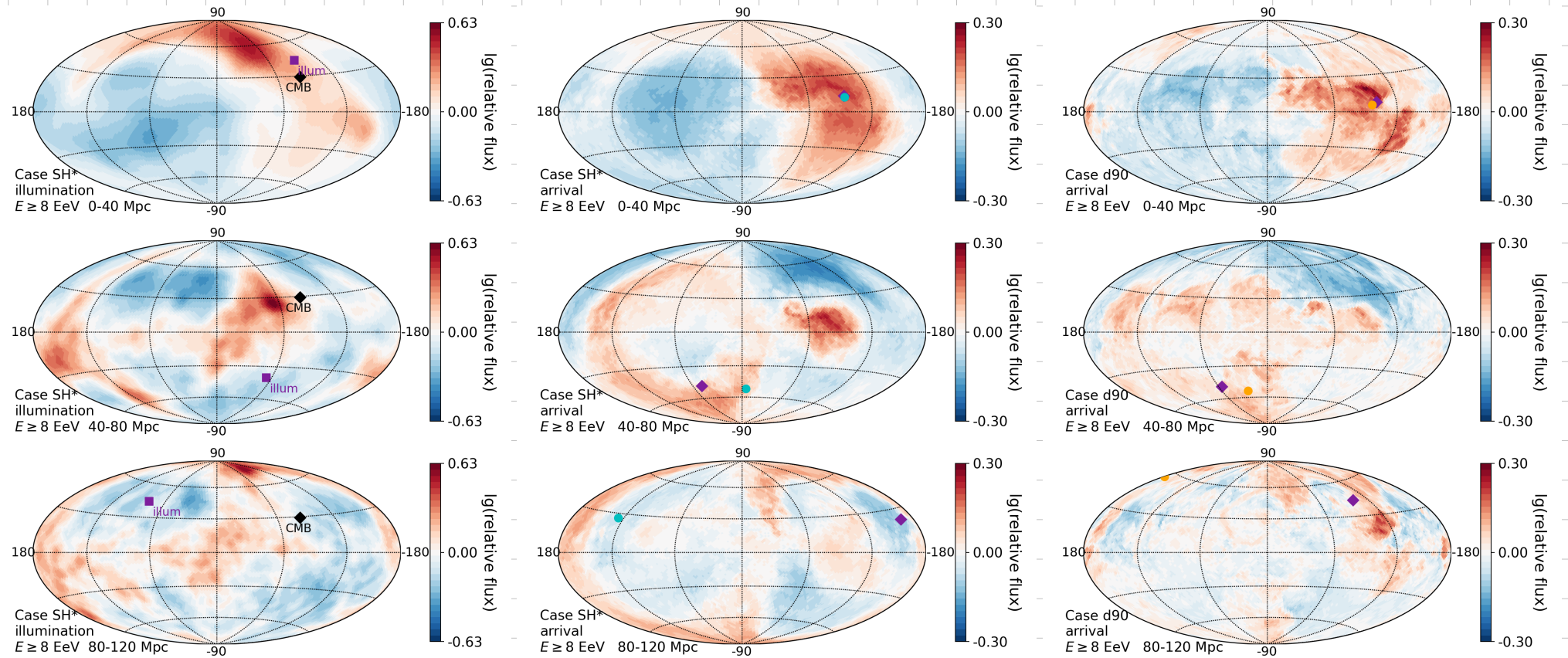
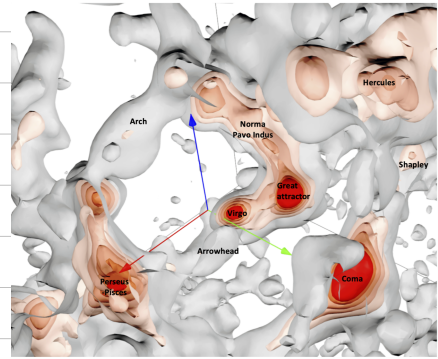


Figure 2. Surface density maps (left column), and arrival maps after propagation in the JF12 Galactic magnetic field model for the SH* (middle) and d90 (right) attenuation models, in LSS shells covering distances (top to bottom): 0-40, 40-80, and 80-120 Mpc. The maps here are for $E \geq 8$ EeV; plots including $E \geq 32$ EeV and a more complete set of distances and models are given in the Appendix Figs. E4– E7.

AugerPrime

Advent of multihybrid data

